

# Cell-to-cell variability and robustness in S-phase duration from genome replication kinetics

Qing Zhang<sup>1,\*</sup>, Federico Bassetti<sup>2,†</sup>, Marco Gherardi<sup>1,3,‡</sup> and Marco Cosentino Lagomarsino<sup>1,3,4,§</sup>

<sup>1</sup> Sorbonne Universités, UPMC Univ Paris 06, UMR 7238,  
Computational and Quantitative Biology, 15 rue de l'École de Médecine Paris,  
France and <sup>2</sup> Dipartimento di Matematica, Università di Pavia,  
Pavia, Italy <sup>3</sup> IFOM, FIRC Institute of Molecular Oncology,  
Milan, Italy <sup>4</sup> CNRS, UMR 7238, Paris, France

(Dated: November 16, 2018)

Genome replication, a key process for a cell, relies on stochastic initiation by replication origins, causing a variability of replication timing from cell to cell. While stochastic models of eukaryotic replication are widely available, the link between the key parameters and overall replication timing has not been addressed systematically. We use a combined analytical and computational approach to calculate how positions and strength of many origins lead to a given cell-to-cell variability of total duration of the replication of a large region, a chromosome or the entire genome. Specifically, the total replication timing can be framed as an extreme-value problem, since it is due to the last region that replicates in each cell. Our calculations identify two regimes based on the spread between characteristic completion times of all inter-origin regions of a genome. For widely different completion times, timing is set by the single specific region that is typically the last to replicate in all cells. Conversely, when the completion time of all regions are comparable, an extreme-value estimate shows that the cell-to-cell variability of genome replication timing has universal properties. Comparison with available data shows that the replication program of three yeast species falls in this extreme-value regime.

## I. INTRODUCTION

In all living systems, the duration of DNA replication correlates with key cell-cycle features, and is intimately linked with transcription, chromatin structure and genome evolution. Dysfunctional replication kinetics is associated to cancer and found in aging cells. Eukaryotic organisms rely on multiple discrete origins of replication along the DNA [1, 2]. These origins are “licensed” during the G1 phase by origin recognition complexes and MCM helicases, and can initiate replication during S phase [3]. Once one origin is activated (“fires”), a pair of replication forks are assembled and move bidirectionally. In one cell cycle, one origin already activated or passively replicated cannot be activated again [2]. Origins have specific firing rates, possibly connected to the number of bound MCM helicase complexes [4], and their specificity determines the kinetics of replication during S phase, or “replication program”.

To investigate genomic replication kinetics, DNA copy number can be measured with microarray or sequencing, as a function of genome position and time (see, e.g., [5–7]). Based on such high-throughput replication timing data, it is possible to infer origin positions and the key parameters for a mathematical description of the replication process (see, e.g., [5, 8, 9]). Recent methods also allow to extract the same information from free-cycling

cells [10]. The mathematical modeling of genome-wide replication timing data shows that replication kinetics results from the stochastic mechanism of origin firing [3, 6]. In other words, replication timing originates from individual probabilities of origin firing (and their correlations with genome state [11–13]). In such models, firing rate of individual origins determine the kinetic pattern of replication along the chromosomal coordinate, and fork velocity is typically assumed to be nearly constant along the genome (in absence of blockage).

Evidence of this stochasticity directly from single cells (which should give access to relevant correlation patterns) is less abundant. Importantly, replication timing patterns observed in population studies can be explained by stochastic origin firing at the single-cell level [14]. Stochastic activation of origins leads to stochasticity of termination and cell-to-cell variability of the total duration of replication of a chromosome, a genomic region, or the whole S-phase [6], with possible repercussions on the cell cycle. This raises several questions, including how the individual rates and spatial distribution of origins cooperate to generate variability in replication timing, the extent of such variability, and whether it is possible to identify specific regimes or optimization principles in terms of cell-to-cell variability. However, such questions have not been systematically addressed in the available models.

A series of pioneering studies [15, 16] has used techniques of extreme-value theory to derive the distribution of replication times in the particular case where each locus of the genome is a potential origin of replication, as in the embryonic cells of *X. laevis*. These efforts allowed to clarify the possible optimization principles underlying

---

\* qzhang519@gmail.com

† federico.bassetti@unipv.it

‡ gocram@gmail.com

§ marco.cosentino-lagomarsino@upmc.fr

the replication kinetics in such organisms.

Here, we extend this approach to the widely relevant case of discrete origins with fixed positions [2, 17, 18] using a modeling framework for stochastic replication to investigate the cell-to-cell variability of the duration of S-phase (or of the replication of any genomic region such as one chromosome). We use analytical calculations based on extreme-value theory and simulations, employ experimental data to infer replication parameters and identify the main features of empirical origin strengths and positions, and their response to specific changes.

## II. MATERIALS AND METHODS

### A. Model

We make use of a one-dimensional nucleation-growth model [19] of stochastic replication kinetics with discrete origin locations  $x_i$ , similar to models available in the literature [5, 20]. Activation of origins (firing) is stochastic, and is described as a non-stationary Poisson process. The firing rate  $A_i(t)$  of the origin located at  $x_i$  is a function of time,  $A_i(t) = \lambda_i t^\gamma \theta(t)$ , where  $\theta(t)$  is the step function, and  $\lambda_i$  and  $\gamma$  are constants [5, 15, 21]. We assume that the parameter  $\gamma$  and the fork velocity  $v$  are common to all origins, whereas  $\lambda_i$ , which reflects the specific strength of each origin, is origin dependent. The probability density function (PDF)  $f_i(t)$  of the firing time  $t$  for the  $i$ -th origin, given that the origin fires during that replication round, can be obtained as  $f_i(t) = A_i(t) \exp\left(-\int_0^t A_i(\tau) d\tau\right)$ , which gives

$$f_i(t) = \lambda_i t^\gamma \theta(t) \exp\left(-\lambda_i \frac{t^{\gamma+1}}{\gamma+1}\right). \quad (1)$$

When  $\gamma > 0$ , i.e., when the firing rate increases with time,  $f_i(t)$  is a stretched exponential distribution. When  $\gamma = 0$ , the firing rates are constant and the process is stationary, so  $A_i(t) = \lambda_i$  and  $f_i(t) = \lambda_i \theta(t) e^{-\lambda_i t}$ .

Once an origin has fired, replication forks proceed bidirectionally at constant speed, possibly overriding other origins by passive replication. When two forks meet in an inter-origin region, replication of that region is terminated. The length of the  $i$ -th region is defined as  $d_i = x_{i+1} - x_i$ ; the time when its replication is completed is  $T_i$ . The duration of the S phase  $T_S$  is the time needed for all inter-origin regions to be replicated.

### B. Fits

Empirical parameters were inferred through fitting experimental data from refs. [6, 7, 22] on DNA copy number as a function of position and time with the model. The positions of replication origins were obtained directly from the literature and considered fixed [6, 7, 22]. The fits are performed by minimizing the distance between

the replication timing profiles in the model and in the experimental data. This is carried out by updating the global parameters ( $\gamma$  and  $v$ ) and the local parameters ( $\lambda_i$ ,  $i \in \{1, 2, \dots, n\}$ ) iteratively (Appendix A). The parameters from these fits are presented in Supplementary Table S1.

### C. Simulations

Our theoretical calculations (described below) allow to obtain the cell-to-cell variability of  $T_S$  in special regimes. We compare simulations using the complete information on the locations and strengths of all origins fitted from the data, with randomized chromosomes having similar properties. In these randomized chromosomes we consider the inter-origin distances  $d_i$  and the strengths  $\lambda_i$  as independent random variables. They are drawn from probability distributions recapitulating their empirical mean and variability. More precisely, from the fitted parameters we fix the mean  $\langle d \rangle$  and the standard deviation  $\sigma_d$  of the distance, and the mean  $\langle \lambda \rangle$  and the standard deviation  $\sigma_\lambda$  of the strength. The actual distances  $d_i$  and strengths  $\lambda_i$  are then drawn by sampling from two gamma distributions

$$d_i \sim \Gamma\left(\frac{\langle d \rangle^2}{\sigma_d^2}, \frac{\langle d \rangle}{\sigma_d^2}\right), \quad \lambda_i \sim \Gamma\left(\frac{\langle \lambda \rangle^2}{\sigma_\lambda^2}, \frac{\langle \lambda \rangle}{\sigma_\lambda^2}\right). \quad (2)$$

The gamma distribution  $\Gamma(a, b)$  (parametrized in terms of a shape parameter  $a$  and a rate parameter  $b$ ) has PDF  $p(x) \propto x^{a-1} \exp(-bx)$ . It yields positive values, with mean  $a/b$  and variance  $a/b^2$ , and it is the maximum-entropy distribution with fixed mean and fixed mean of the logarithm. We verified that the assumption of a gamma distribution was in line with empirical data (Fig. S1).

To explore the full range of parameters, we also used stochastic simulations, which were performed both (i) with the precise origin locations and strengths fitted from the data, and (ii) with  $d_i$  and  $\lambda_i$  drawn randomly as described above. To avoid the boundary effects of linear chromosomes, we consider circular chromosomes with  $n$  origins, unless specified otherwise (boundary effects are discussed in the Appendix B and Fig. S2, and do not affect our main conclusions.)

To analyze the biologically relevant regimes, we considered replication kinetics data on different yeast species, from refs. [6] and [7], ran simulations with such parameters, and compared with the theoretical predictions using the empirical values for  $\sigma_d$ ,  $\sigma_\lambda$  and mean origin positions and strengths.

### III. BACKGROUND

#### A. The S-phase duration is the result of a maximum operation on the stochastic replication times of inter-origins regions

We start by discussing how the stochastic nature of single-origin firing affects the total replication timing of a chromosome. Fig. 1ab illustrates this process. In each cell, a chromosome is fully replicated when the last inter-origin region is complete. In other words, the last-replicated region sets the completion time for the whole chromosome. Consequently, the total duration is the maximum among the replication times of all inter-origin regions [16]. For simplicity, we first consider the case of a genome with only one chromosome. The duration of the S phase is therefore  $T_S = \max(T_1, T_2, \dots, T_n)$  where  $n$  is the number of inter-origin regions. The stochasticity of the replication time  $T_i$  of each inter-origin region makes the S-phase duration  $T_S$  itself stochastic, thus giving rise to cell-to-cell variability, which can be estimated by the model (Fig. 1c). In the case of multiple chromosomes, the same reasoning applies to the last-replicated inter-origin region over all chromosomes.

### IV. RESULTS

#### A. A theoretical calculation reveals the existence of two distinct regimes for the replication program

It is possible to estimate the distribution of  $T_S$  analytically, starting from the distribution of  $T_i$ . Two distinct limit-case scenarios can be distinguished. In the first scenario, a specific inter-origin region  $r$  is typically the slowest to complete replication and thus represents a “replication bottleneck”. In this case,  $T_S$  is dominated by  $T_r$ , meaning that  $T_S \approx T_r$ .  $T_r$  is identified as the one which is largest on average. Fig. S5a shows an example chromosome with 10 origins with the same strength, where one inter-origin distance ( $d_1$ ) is much larger than the others. Owing to this disparity,  $T_1$  is very likely the maximum among all  $T_i$ , and is therefore the region determining  $T_S$ . In this scenario, which we term “bottleneck estimate”, the distribution of  $T_S$  will be approximately the same as that of the bottleneck  $T_r$  (Fig. S5c).

In the second scenario, each inter-origin region has a similar probability to be the latest to complete replication. In this case, every inter-origin region contributes to the distribution of  $T_S$ . Since  $T_S = \max(T_1, T_2, \dots, T_n)$ , we apply the well-known Fisher-Tippett-Gnedenko theorem [23, 24], which is a general result on extreme-value distributions (EVD). In order to use this theorem, we make the following two assumptions: (i)  $T_1, T_2, \dots, T_n$  are statistically independent, i.e., each inter-origin replication time is an independent random variable, incorporating the essential information about origin variability and rates; (ii)  $T_i$  follows a stretched-exponential distribution, independent of  $i$ , i.e.

$$p(T_i < t) = 1 - e^{-\alpha(t-t_0)^\beta}, \quad (3)$$

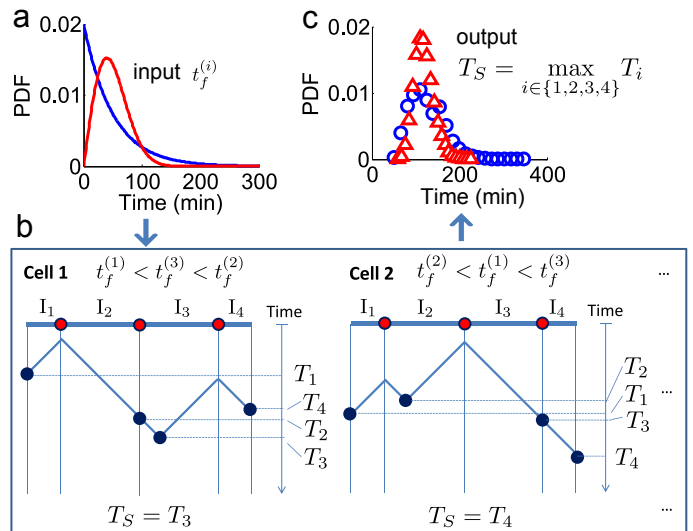


FIG. 1. **The S-phase duration is the maximum between the stochastic termination time of all inter-origin regions.** The illustration considers replication of one linear chromosome with three origins. (a) The activation of each origin is stochastic, and the firing time  $t_f^{(i)}$  follows a given phenomenological distribution. (b) In each cell, each origin randomly chooses a firing time from this distribution. The last replicated inter-origin region, which may be different in different cells, determines the total duration of the S phase. In the sketch, red circles indicate origins. Dark blue circles indicate the latest replicated loci for each inter-origin region. Some origins (e.g., the one between  $I_2$  and  $I_3$  in cell 1) may be replicated passively, and never fire in some realization. (c) The stochastic model generates a distribution of S-phase durations, which expresses the cell-to-cell variability. The parameters used in the plots are: chromosome length  $L = 300kb$ , fork velocity  $v = 1kb/min$ , firing exponent  $\gamma = 0$  (blue line in (a) and blue circles in (c)) or 1 (red line in (a) and red triangles in (c)), origin locations  $x_1 = 50 kb$ ,  $x_2 = 150 kb$  and  $x_3 = 250 kb$ , origin strength  $\lambda_{1,2,3} = 0.02 \text{ min}^{-1}$  (for  $\gamma = 0$ ) or  $6.3 \times 10^{-4} \text{ min}^{-2}$  (for  $\gamma = 1$ ).

bution, independent of  $i$ , i.e.

when  $t > t_0$ , while  $p(T_i < t) = 0$  when  $t \leq t_0$ . The (positive) parameters  $\alpha$ ,  $\beta$  and  $t_0$ , effectively describe the consequences of the model parameters  $v$ ,  $\gamma$ , inter-origin distances ( $d_1, d_2, \dots, d_n$ ) and origin strengths ( $\lambda_1, \lambda_2, \dots, \lambda_n$ ) on completion timing of inter-origin regions (see below and Appendix D), and can be obtained by fitting the distribution of replication time for a typical inter-origin region (obtained from simulations) with Eq. 3.

Our fits show that Eq. 3 is a remarkably good phenomenological approximation of the distribution of  $T_i$  (see Appendix C and Fig. S3), thus justifying assumption (ii) above. Note that the fitted stretched exponential form also incorporates effectively the coupling existing between different inter-origin regions. Indeed,

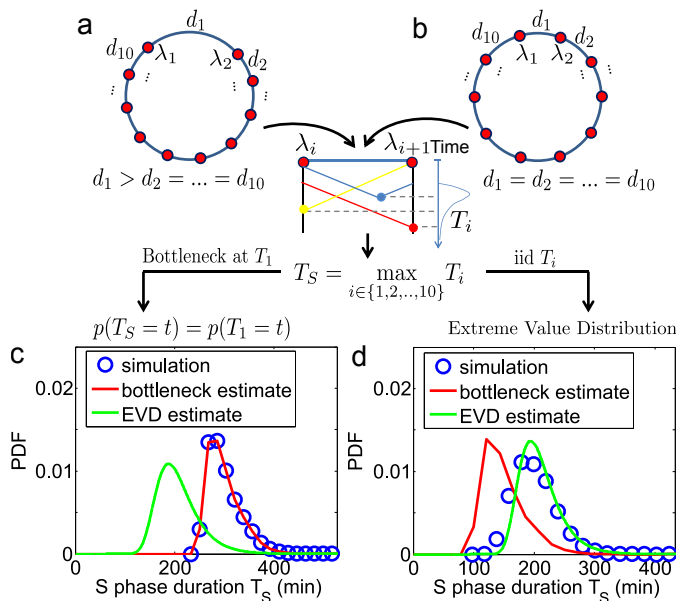


FIG. 2. **Analytical estimates indicate the existence of two replication regimes.** (a) If a single “bottleneck” inter-origin region (labelled by the index 1 in panels a and b) is typically the last to complete replication,  $T_S$  will be typically equal to  $T_1$  (inter-origin distances in the example are  $d_i = 167 \text{ kb}$  for all origins except  $d_1 = 500 \text{ kb}$ ). (b) If the replication times of all inter-origin regions are comparable, and they are considered independent and identically-distributed (iid) random variables, the distribution of  $T_S$  can be obtained by extreme-value-distribution (EVD) theory (inter-origin distances are  $d_i = 200 \text{ kb}$ ). Simulations of the model (blue circles), when one inter-origin distance is much larger than the others (c), and when all inter-origin distances and strengths are comparable (d), agree with the corresponding analytical calculations (red and green curves). (Origin number  $n = 10$  origins, fork velocity  $v = 1 \text{ kb/min}$ , origin strength  $\lambda_i = 0.02 \text{ min}^{-1}$ .)

neighboring regions are correlated since they use a pair of replication forks stemming from their common origin. Moreover, even distant inter-origin regions can share the same fork if they are passively replicated. In order to justify the assumption (i), we tested the effect of the correlation between different regions, by sampling  $T_1, T_2, \dots, T_n$  from the distribution in Eq. 3 independently and then taking their maximum  $T_S^*$ . We verified that the difference between the distribution of  $T_S^*$  and that of  $T_S$  obtained from simulation (where the correlations are present) is small. Therefore, the effect of these relatively short-ranged correlations can be, to a first approximation, neglected at the scale of the chromosomes and of the genome, and described by the effective stretched-exponential form (see Fig. S4).

Based on these assumptions, we can use the Fisher-Tippett-Gnedenko theorem and derive the following cumulative distribution function for  $T_S$  as a function of the number of origins  $n$  and the parameters  $\alpha$ ,  $\beta$  and  $t_0$  (the

calculation is detailed in the Appendix D):

$$P(T_S \leq t) \approx \exp \left\{ - \exp \left[ \beta \log n \left( 1 - (\alpha / \log n)^{1/\beta} (t - t_0) \right) \right] \right\}. \quad (4)$$

Eq. 4 gives a direct estimate of the distribution of the S-phase duration in this second scenario, which we term “extreme-value” or “EVD” regime. The resulting distribution is universal, since it does not depend on the detailed positions and rates of the origins, and depends in a simple way on the parameters  $\alpha$ ,  $\beta$ ,  $t_0$  and  $n$ . Although the extreme-value estimate should apply to the case of large  $n$ , the approximation Eq. 4 holds to a satisfactory extent also for realistic values, when  $n$  is order 10 (see Supplementary Fig. S12). We also derived approximate analytical expressions for  $\alpha$ ,  $\beta$  and  $t_0$  as functions of the parameters  $v$ ,  $\gamma$ , for a “typical” region characterized by  $\langle \lambda \rangle$  and  $\langle d \rangle$  under the assumption of negligible interference from non-neighbour origins (see Appendix D).

The procedure by which we apply Eqs. 3 and 4 is the following. Given inter-origin distances and origins strengths assigned arbitrarily or inferred from empirical data, the simulation of the replication of a chromosome gives the distribution of  $T_i$  and  $T_S$ . A fit of the distribution of  $T_i$  from simulation using Eq. 3 gives the parameters  $\alpha$ ,  $\beta$  and  $t_0$ . Finally, the EVD estimate for the distribution of  $T_S$ , can be obtained from Eq. 4, and compared with the distribution of  $T_S$  from simulations. This procedure can be seen as a variant of the method introduced in refs. [15, 16] applicable to the case of discrete origins (see Discussion).

Fig. S5b shows one example where one circular chromosome has 10 origins with identical strengths and identical inter-origin distances. The estimated distribution of S-phase duration from Eq. 4 is well-matched with the simulated one (Fig. S5d). Fig. S5 also shows how the bottleneck estimate works for the opposite scenario, and compares simulations with both estimates in the two different regimes. Similar to Fig. S5, Supplementary Fig. S5 shows the existence of the two regimes in presence of a single origin affecting the two neighboring inter-origin regions. In the bottleneck regime, these two regions replicate much later than the others, because their common origin is much weaker than the other origins; the S-phase duration is then dominated by their replication time. This case also illustrates how the bottleneck regime may not be limited to a single inter-origin region. Finally, Supplementary Fig. S6 shows the distribution of the inter-origin completion times  $T_i$  in the cases presented in Fig. S5 and Supplementary Fig. S5. This analysis illustrates how extra peaks in the right tail of  $T_i$  distribution relate to the failure of the extreme-value estimate for the distribution of S-phase duration. These examples indicate that, as expected, the presence of outliers in the values of  $T_i$  (exceedingly slowly-replicating regions) is responsible for the onset of the bottleneck behavior.

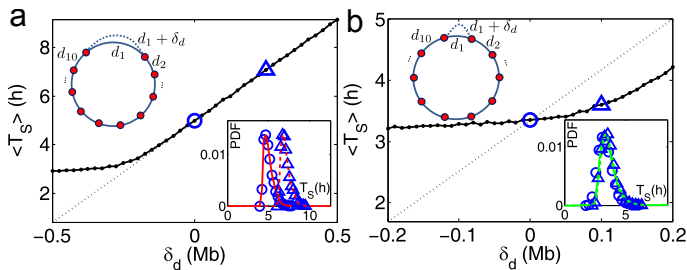


**FIG. 3. Effects of perturbations of a single inter-origin region on S-phase duration.** (a) The bottleneck inter-origin region of the chromosome shown in Fig. S5a is perturbed by increasing its length by  $\delta_d$  (i.e.,  $d_1 \rightarrow d_1 + \delta_d$ ). The black solid line with points is the average S-phase duration, which increases linearly with  $\delta_d$ . The black dotted line, with slope  $1/(2v)$ , is a guide to the eye. The inset shows that the perturbation shifts the distribution of  $T_S$  by  $\delta_d/2v$  (circles are simulations for the unperturbed chromosome, and triangles correspond to  $\delta_d = d_1/2$ ; the two curves are the analytical estimates in the bottleneck regime). (b) The same perturbation as in (a) is performed on an inter-origin region of the chromosome shown in Fig. S5b, which lies in the EVD regime. Symbols are as in (a). The distribution of  $T_S$  is robust to this perturbation.

### B. The extreme-value regime is robust to perturbations increasing the replication timing of a local region

Origin number, origin strengths and inter-origin distances can be perturbed due to genetic change (DNA mutation or recombination), over evolution, and due to epigenetic effects such as binding of specific agents. We can compare the robustness of the two regimes identified above to perturbations of these parameters. We consider in particular the elongation of a single inter-origin distance  $d_i \mapsto d_i + \delta_d$  (similar results to those reported below are obtained for a perturbation affecting the strength of a single origin, see Supplementary Fig. S7). In such case, the change of  $T_i$  is approximately equal to  $\delta_d/2v$ . In the bottleneck regime, if the perturbed inter-origin region is the slowest-replicating one,  $\langle T_S \rangle$  increases linearly with  $\delta_d$  with slope  $1/2v$ , and the distribution of  $T_S$  shifts by a delay  $\delta_d/2v$  (Fig. S7a). In the extreme-value regime, instead, there is no single bottleneck inter-origin region, and the change of  $T_S$  with the perturbation turns out to be much smaller than  $\delta_d/2v$  (Fig. S7b). Notice that in both regimes the variability of the S-phase duration around its average is not affected sensibly (insets of Fig. S7).

In summary, the bottleneck region is “sensitive” to the specific perturbations considered, since termination of replication is highly dependent on a single inter-origin region, while the EVD regime is “robust”, as the effect of small local perturbations can be absorbed by passive replication from nearby origins [6].

### C. Diversity between completion times of inter-origin regions sets the regime of the replication program

The cases discussed above (Fig. S5) recapitulate the expected behavior in case of high versus small variability of the typical completion time of different inter-origin regions. One can expect that if the variability of the inter-origin distances is large, or origin strengths are heterogeneous, it will be more likely to produce a bottleneck region, which in turn will trivially affect replication timing. Conversely, the replication program will be in the extreme-value regime if the completion times of all regions are comparable. In order to show this, we tested systematically how average and variability of  $T_S$  change with the variability of inter-origin distances and origin strengths in randomly generated genomes. In this analysis, origin spacings and strengths are assigned according to the prescribed probability distributions shown in Eq. 2, with varying parameters (see the Methods for a precise description of how chromosomes are generated).

Fig. 4 shows the results. Importantly, we find that the regimes defined above as extreme cases apply for most parameter sets, and there is only a small region of the parameters where we find intermediate cases. Specifically, two parameters, the standard deviations  $\sigma_d$  and  $\sigma_\lambda$ , of the inter-origins distances and the origin strengths respectively, are sufficient to characterize the system. Fig. 4a indicates that as long as  $\sigma_d$  is smaller than a threshold (around 30 kb), the average  $\langle T_S \rangle$  and the standard deviation  $\sigma(T_S)$  of the replication time are approximately constant. In this regime, the extreme-value estimate matches well the simulation results. When  $\sigma_d$  exceeds the threshold, the average of  $T_S$  increases and its standard deviation decreases with large fluctuations. In this other regime, both  $\langle T_S \rangle$  and  $\sigma(T_S)$  deviate from the EVD estimate. Fig. 4b shows that varying  $\sigma_\lambda$  at fixed origin positions produces a similar behavior (although with smaller deviations from the EVD estimates).

This analysis shows an emergent dichotomy between these two regimes, which depends on the distribution of  $T_i$  (i.e. both inter-origin distances and origin firing rates). In principle, more complex situations where e.g. a subset of many comparably “slow” inter-origin regions dominates S-phase timing is possible, but this situation is very rare (and negligible) if origin rates and positions are generated with the criteria used here (given by Eq. 2). *De facto*, under these prescriptions, motivated by empirical properties of origin positions and strengths, only the two regimes defined above as extreme cases were observable. For example, one can imagine a situation where each chromosome are, separately, in the EVD regime, but the replication of one of the chromosomes takes considerably longer than the others on average, which may lead the S-phase duration to be in the bottleneck regime. However, we find that this situation is essentially never found if origin rates and positions have empirically relevant values (i.e. for all realizations with empirical means

and variances of inter-origin distances and origin firing rates). Qualitatively, this will always be the case if the distribution of  $T_i$  shows a single mode, and there are very few, or just one exceptional late-replicating region.

This behavior suggests to define “critical values” of  $\sigma_d$  and  $\sigma_\lambda$ , separating the extreme-value regime from the bottleneck regime, as follows. We define the  $\sigma_d^c$ , at fixed  $\sigma_\lambda$ , as the value of  $\sigma_d$  at which  $\langle T_S \rangle$  (possibly averaged over many samples of the origin configuration too, denoted  $\langle\langle T_S \rangle\rangle$ ) is 20% larger than at  $\sigma_d = 0$  and  $\sigma_\lambda = 0$ . The results presented here do not depend appreciably on this threshold and do not change much if we define  $\sigma_d^c$  as the value of  $\sigma_d$  at which  $\langle T_S \rangle$  is 20% off the prediction of the EVD theory. The same definition holds for  $\sigma_\lambda^c$  at fixed  $\sigma_d$ . Surprisingly,  $\sigma_d^c$  turns out to be independent of  $\sigma_\lambda$ , and  $\sigma_\lambda^c$  independent of  $\sigma_d$ . The resulting “phase diagram”, shown in Fig. 4c, separates the space of parameters into an approximately rectangular region where the EVD estimate is precise, and an outer region where heterogeneities dominate, which is identified with the bottleneck regime.

We can give a simple argument for why this phase diagram is approximately rectangle-shaped. Intuitively, a large  $\sigma_d$  increases the probability of extracting a very large value for  $d$ , and a large  $\sigma_\lambda$  increases the probability of extracting a very small  $\lambda$ . In a realization of a randomized chromosome, such rare events may generate an extremely slow-replicating region acting as the bottleneck. Clearly, drawing an extreme value for only one of the two variables is sufficient to generate the bottleneck region, giving rise to the two sides of the rectangle. For values of the variances of both variables that are below the individual thresholds, drawing a large  $d$  and small  $\lambda$  jointly makes the upper-right region of the rectangle rounded. However, such joint extreme draws in the same inter-origin region are very rare, because the two variables are drawn independently, so the rounded upper-right corner is very small, as visible in Fig. 4c.

#### D. The yeast replication program is just inside the EVD regime and likely under selection for short S-phase duration

The results of the previous section indicate that the standard deviations of the origin distances and of the strengths are the most relevant parameters determining the regime of the distribution of the S-phase duration across cells. We inferred the parameters from replication timing data of the yeasts *S. cerevisiae* (ref. [6]), *L. kluyveri* (ref. [7]) and *S. pombe* (ref. [22]). Such fits fully constrain the model parameters: fork velocity  $v$ ,  $\gamma$ , start of the S phase  $t_0$ , origin strengths  $\lambda_i$  and inter-origin distances  $d_i$ , from which we calculated  $\langle d \rangle$ ,  $\langle \lambda \rangle$ ,  $\sigma_d$  and  $\sigma_\lambda$ , and simulated the duration of S phase and replication time of each chromosome (see Appendix A and Fig. S8-10). In these simulations we consider circular chromosomes with  $n$  origins, and boundary effects are

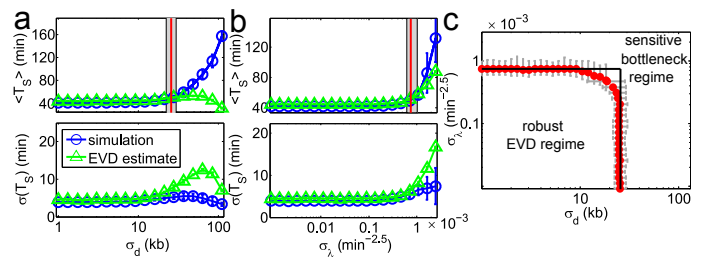


FIG. 4. **The variabilities of the inter-origin distances,  $\sigma_d$ , and of the firing strengths,  $\sigma_\lambda$ , set the replication regime.** (a,b) Average S phase duration (top panels) and its standard deviation (bottom panel) as functions of  $\sigma_d$  (panel a) or  $\sigma_\lambda$  (panel b), obtained by simulations of the model (blue circles and lines) and by the EVD estimate (green triangles and lines). 50 samples of inter-origin distances and origin strengths are chosen according to the distributions in Eq. (2). Red lines indicate the transition points where the simulated  $\langle\langle T_S \rangle\rangle$  is 20% larger than at  $\sigma_d = 0$  and  $\sigma_\lambda = 0$ . The border lines of the grey area show the transition points for  $\langle\langle T_S \rangle\rangle + \sigma(\langle T_S \rangle)$  and  $\langle\langle T_S \rangle\rangle - \sigma(\langle T_S \rangle)$  respectively. (c) Phase diagram separating the EVD and bottleneck regimes. Red transition points with error bars (obtained with the method shown in (a) and (b)) form an approximate rectangle phase boundary. Parameters: fork velocity  $v = 1.81$  kb/min, origin number  $n = 20$ ,  $\gamma = 1.5$ ,  $\langle d \rangle = 28.13$  kb,  $\langle \lambda \rangle = 6.17 \times 10^{-4}$  min<sup>-2.5</sup>,  $\sigma_\lambda = 0$  (a) and  $\sigma_d = 0$  (b).

tested in the Appendix B and Fig. S2, and do not affect our main conclusions, indicating that, according to the model, the partition of the genome into 16 unconnected chromosomes has little effect on the statistics of S-phase duration. The values of  $\gamma$  that were obtained as best fits of the empirical data (Supplementary Fig. S8) were in line with previous analyses (e.g. [5, 6]). In addition, we found that the standard deviation of the predicted S-phase duration decreases with the parameter  $\gamma$  (Supplementary Fig. S9), which agrees with the finding of previous studies focused on *X. laevis* [15, 16].

This analysis indicates that the whole-genome values of  $\sigma_d$  and  $\sigma_\lambda$  measured for *S. cerevisiae*, *L. kluyveri* and *S. pombe* place these genomes within the extreme-value regime. Rescaling  $\sigma_d$  and  $\sigma_\lambda$  by the crossover values  $\sigma_d^c$  and  $\sigma_\lambda^c$  respectively makes it possible to compare data with different mean  $T_S$ . This comparison (Fig. 5a) shows that not only the genomic but also most of chromosomal parameters of *L. kluyveri*, *S. cerevisiae* and *S. pombe* are located in the extreme-value regime. With the fitted parameters, most of chromosomes and genomes are found in the extreme-value regime (as an example, see Supplementary Fig. S10). Interestingly, all chromosomes (and the full genome) lie close to the transition line. This may be a consequence of the presence of competing optimization goals, such as replication speed (or reliability) and resource consumption by the replication machinery [16].

Furthermore, we considered data of two *S. cerevisiae* mutants. In one mutant, three specific origins in three different chromosomes (6, 7, and 10) were inactivated [6].

The inactivation of a specific origin slows down the replication of the nearby region, which might cause a bottleneck. Our results show that this origin mutant is still in EVD regime (Supplementary Fig. S13). Importantly, in this case the model should be able to make a precise prediction for the replication profile of the chromosomes where one origin is inactivated. Supplementary Fig. S14 shows the prediction on the replication profile of origin mutant strain based on the parameters fitted from the data of wild-type strain (except that the three inactivated origins are deleted from the origin list). The model prediction is in fairly good agreement with data. The mismatch between prediction and data in some regions (but not others) is an interesting feature revealed by the model, and may result from experimental error or gene-expression adaptation of the mutants [6]. The other mutant strain that we considered is *isw2/nhp10*, from the study of Vincent and coworkers [25], who analyzed the functional roles of the Isw2 and Ino80 complexes in DNA replication kinetics under stress. This study compares the behavior of wild type (wt) strain and a *isw2/nhp10* mutant in the presence of MMS (DNA alkylating agent methyl methanesulfonate) and found that S-phase in *isw2/nhp10* is extended compared to the wt strain because the Isw2 and Ino80 complexes facilitate replication in late-replicating-regions and improve replication fork velocity. In agreement with these findings, the model fit of the data shows that *isw2/nhp10* mutant has more inactive origins and smaller fork velocity. Such conditions may facilitate the onset of a bottleneck regime in the mutant compared to the wt strain. We found that *S. cerevisiae* wt strain treated with MMS still falls in the extreme-value regime. Conversely, some chromosomes (e.g 13 and 15) of the *isw2/nhp10* mutant are in the bottleneck regime, and in this case, the whole genome (entire S-phase), is driven in the bottleneck regime (see Supplementary Fig. S15). Strikingly, the model makes a good prediction on the replication profile of the *isw2/nhp10* mutant, using origin firing strengths and the  $\gamma$  values fitted from the wild-type strain experiments, and just adjusting two (global) parameters replication speed and an overall factor in all origin firing rates (Supplementary Fig. S16). This provides a good cross-validation of the applicability of the model in a predictive framework.

A further question is whether we can detect signs of optimization in the duration of chromosome replication. Fig. 5b compare the S-phase durations obtained from simulations of the model in two cases: (i) by using the origin positions and strengths from empirical data (see Supplementary Fig. S10), and (ii) by using a null model with randomized parameters (both origin strengths and inter-origin distances) drawn according to Eq. (2), and preserving the empirical mean and variance. The results show that for some of the chromosomes the average replication timing  $T_S$  is close to the typical one obtained from randomized origins (e.g., chromosomes 1,3,5,6,8,11,13 in *S. cerevisiae*). For other chromosomes

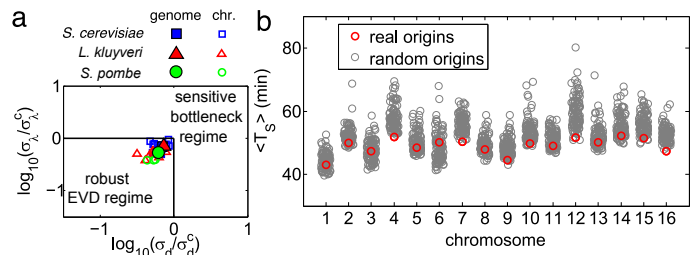


FIG. 5. **The replication program of yeast is in the robust regime.** (a) Symbols are the parameters of *S. cerevisiae* (blue squares), *L. kluyveri* (red triangles) and *S. pombe* (green circles), inferred from fits with replication timing data from [6], [7] and [22] respectively (see Supplementary Table S1). Filled symbols correspond to the whole genome, hollow symbols to each chromosome. (b) For each chromosome of *S. cerevisiae*, the average S-phase duration (y axis) is compared (by simulations of the model) between empirical origin positions and firing strengths (red circles) and randomized origins with empirically fixed distributions (grey circles).

(e.g., 2,4,7,10,12,15,16 in *S. cerevisiae*) the empirical average  $T_S$  is instead very close to the minimum reachable within their ensemble of randomizations. Remarkably, chromosomes with higher average replication timing in the randomized ensemble seem to be more subject to pressure towards decreasing their average  $T_S$  (Supplementary Fig. S11). This result suggests that the whole replication program may be under selective pressure for fast replication.

## V. DISCUSSION

The core of our results are analytical estimates that capture the cell-to-cell variability in S-phase duration based on the measurable parameters of replication kinetics. Extreme-value statistics has been applied to DNA replication before [15, 16], but only to the case of organisms like *X. laevis*, where origin positions are not fixed and there is no spatial variability of initiation rates. To our knowledge, this method has not been applied systematically to fixed-origin organisms such as yeast. More specifically ref. [15] explores the case of a perfect lattice of equally spaced discrete origins with fixed and equal firing rates, but does not address the role of the variability of inter-origin replication times due to randomness in firing rates and inter-origin distance, which is relevant for fixed-origin organisms. Another difference is that the authors of ref. [15, 16] derive the coalescence distribution starting from their model, while here we assume a stretched-exponential, motivated by data analysis. Since their distribution is more complex (although the model is simpler), EVD estimate leads to a formula linking the parameters of the Gumbel distribution to the initiation parameters in the form of an implicit equation, that needs to be solved numerically. Conversely, the assumption

that the shape of the distribution of  $T_i$  is given (and estimated from data), gives an explicit relationship between the parameters describing the  $T_i$  distribution and the Gumbel parameters, leading to simpler formulas and applicability to the case of discrete origins with different spacings and firing rates. The parameters of the  $T_i$  distribution have then to be related to the microscopic parameters (See Appendix D).

It is important to note that an approach based on extreme-value distribution theory is general [16]. Simulations (including the model used here) are based on specific assumptions that are often not simple to test and many models on the market use slightly different assumptions. Instead, the extreme-value estimates are robust to different shades of assumptions used in the models available in the literature, and thus more comprehensive. Our estimates reveal universal behavior in the distribution of S-phase duration. There is a prescribed relation between mean and variance of S-phase duration, defining a “scaling” behavior for its distribution. Such universality has been observed in cell-cycle periods and cell size [26, 27]. Qualitatively, we expect the same universality to hold in a regime when origins have less than 100% efficiencies, and some may not fire at all during S-phase. Origins that fire only in a fraction of the realizations are accounted for in our simulations, but they entail second-neighbour effects that are not currently accounted in our estimates.

There are hundreds of origins in a genome, but our analysis shows that the relevant parameters to capture the overall behavior are the means and variances of inter-origin distances and origin firing rates. Specifically, we find that two regimes describe most of the phenomenology, and they depend on the values of these effective variables. Importantly, the regimes identified here differ from those identified in ref. [15], which just identify a critical spacing between discrete (equally spaced) origins, for which replication timing starts to be linear with inter-origin distance.

The notion that the last regions to replicate may tend to be different in every cell (our “extreme-value” regime) has been proposed already by Hawkins and coworkers [6]. The opposite regime where some specific regions tend to always replicate last (‘bottleneck region’), has been proposed for mammalian common fragile sites [28]. Such regions of slow replication, pausing and frequent termination have also been described in yeast [6, 29–31]. These studies make it plausible to think that both extreme-value and bottleneck regimes may apply to yeast, despite our analysis based on replication kinetics data indicating some pressure towards the extreme-value regime. Another important case for what concerns replication termination is the rDNA locus, which cannot be analyzed in replication kinetics data based on microarrays / sequencing data due to its repetitive nature ( $\sim 150$  identical copies in yeast). However, the large inter-origin distances, pseudo-unidirectional replication and epigenetic control of origin firing in this locus [32] make it a good

candidate for the last sequence to replicate in yeast.

Importantly the model used here is similar to a set of previous studies, which have tested this approach and validated it with experimental data [3, 5, 6, 8, 15, 33]. Our analysis of S-phase duration in single cells is generic, and expected to be robust to variations model details. The mutant data sets analyzed here also support the predictive power of the model in presence of perturbations and parameter changes, and hence validate the use of the model in a predictive framework. Our predictions are compatible with the available values for average S-phase duration, which can be roughly estimated through flow cytometry [6, 7], and corresponds well to the values obtained by the model (around 60 minutes for *S. cerevisiae*). Other yeast studies found smaller values in other conditions [34], which would be interesting to study with the model. Additionally, we provide a prediction for the cell-to-cell variability of S-phase duration, which is an important step of the cell cycle. Indeed, completion of replication needs to be coordinated with growth and progression of the cell cycle stages [35, 36]. Cell-to-cell variability in replication kinetics makes the S phase subject to inherent stochasticity. Experimentally, measuring the cell-to-cell variation of the S-phase duration is a challenge. While some studies exist using mammalian (cancer) cell lines [37], they currently do not have the precision needed to allow a quantitative match with models. However, we expect that such measurements will become available in the near future, thanks to rapidly developing methods of single-cell biology [38]. Our predictions define some key properties of the replication period that may be tested with, e.g., single-cell studies in budding yeast, using the parameters available from replication kinetics studies. In this model the S phase is (by itself) a “timer”, so its connection to cell size homeostasis must be affected by external mechanisms [35]. S-phase duration has been measured on single *E. coli* cells, and found to be unlinked to cell size [39]. Interestingly, our predictions of S-phase duration and variability as a function of chromosome copy numbers (Supplementary Fig. S12) might apply to cancer cell lines with different levels of aneuploidy [37]. Finally, there is the possibility of applying this framework to describe relevant perturbations [40, 41]. This could also help elucidate how response to DNA damage affects the replication timing and its variability across cells.

Intriguingly, we also found evidence of bias towards faster replication in empirical chromosomes compared to randomized ones. Thus, our overall findings support the hypothesis of a possible selective pressure for faster replication, and against bottlenecks. Other approaches have assumed optimization for faster replication and looked for optimal origin placement [42] or found other signs of optimality in similar data [5]. Our results are in line with these findings, and isolate a complementary direction for such optimization. All these considerations support the biological importance of replication timing of inter-origin regions and its variability. However, the sources of the constraints remain an open question. Clearly, overall



replication speed can increase indefinitely by increasing origin number and initiation rates. However, there are likely yet-to-be-characterized tradeoffs in these quantities, that prevent this from happening, and force the system to optimize the duration of replication in a smaller space of parameters. The molecular basis for such constraints likely lies at least in part in the finite resources available for initiation complexes [4].

## ACKNOWLEDGMENTS

We are grateful to Gilles Fischer, Nicolas Agier, Alessandra Carbone and Renaud Dessalles for useful discussions. QZ was supported by the LabEx CALSIMLAB, public grant ANR-11-LABX-0037-01 constituting a part of the ‘‘Investissements d’Avenir’’ program (reference : ANR-11-IDEX-0004-02; YK).

### Appendix A: Fitting replication timing data from experiments using the model

This section describes our fitting procedure based on the model. The fitted parameters were used in simulations of genome replication kinetics can giving the distribution of S-phase duration and of replication time of one chromosome (Fig. S10).

We used flow cytometry (FACS) data to re-normalize replication timing as follows. If the base line value of average DNA copy-number  $a$  is remarkably larger than 1, and/or its plateau value  $b$  is remarkably smaller than 2, we use the formula  $y = a + \frac{(b-a)(t-T_0)^r}{(t-T_0)^r + (t_c-T_0)^r} \theta(t-T_0)$  to fit the FACS data and normalize replication timing data by  $\phi_{\text{norm}}(x, t) = 1 + \frac{\phi(x, t) - a}{b - a}$ , where  $\phi$  is the replication probability function [7].

We used fixed origin locations from the literature and optimized the fit for the parameters  $\gamma$ ,  $T_0$ ,  $v$  and  $\lambda_i$  iteratively. The objective function was defined as the L2 distance (the average of squared differences) of the experimental and theoretical replication probability timing profile (Fig. S10), i.e., as  $\sqrt{\sum_i \sum_j (\phi_{\text{model}}(x_i, t_j) - \phi_{\text{exp.}}(x_i, t_j))^2 / (N_x N_t)}$ , where  $N_x$  and  $N_t$  are the numbers of the measured loci and time points respectively.

Initialization of the parameters for the fits was performed as follows. Firing rate exponent  $\gamma$  and fork velocity  $v$  were initialized at arbitrary values (typically  $\gamma$  at 0,  $v$  at 2 kb/min). The start of S phase  $T_0$  was initially set when genome copy number from the normalized FACS data (from the interval  $[a, b]$  to  $[1, 2]$ ) is first larger than a fixed threshold (e.g. 1.05) and each origin strength  $\lambda_i$  starts from the value fitted with the time-course data at this origin.

Fitting was performed with following iterative rule. 1) for a parameter  $x$ , assume it has a step length  $\Delta_x$ , and a memorized step length  $\Delta'_x = 2\Delta_x$ , 2) set  $r = \Delta_x / \Delta'_x$

and  $\Delta'_x = \Delta_x$ , if  $x + \Delta_x$  gives a better fit than  $x$ , let  $x = x + \Delta_x$ , otherwise (i) if  $|r| = 1$ , we update  $\Delta_x \rightarrow \Delta_x / 2$  (ii) if  $|r| = 0.5$ , set  $\Delta_x \rightarrow -\Delta_x$ ; 3) repeat 2) until the termination condition is satisfied.  $\lambda_1, \lambda_2, \dots, \lambda_n$  for each chromosome are updated iteratively given  $\gamma$ ,  $v$  and  $T_0$  and in each iteration, one  $\lambda_i$  is chosen randomly to be updated.  $T_0$  is updated iteratively given  $\gamma$  and  $v$ .  $v$  is updated iteratively given  $\gamma$ . For  $\gamma$ , we tested some discrete values between 0 and 3. Supplementary Fig. S8a,b indicate the best fit value of  $\gamma$  for *S.cerevisiae* and *L.kluiveri*, and Supplementary Fig. S8c shows one example of the best fit.

### Appendix B: Role of chromosome boundaries in replication timing

In some simulations, we used circularized chromosomes for easier comparison with the analytical estimates, but relative to a circular chromosome, a linear chromosome has lower symmetry because of the boundary at both ends. To verify that this assumption does not qualitatively affect the results, we circularized the empirical *S.cerevisiae* chromosomes by linking their ends respectively, and simulated their replication kinetics with the estimated parameters. The results (Fig. S2) show that the circularized chromosomes always replicate faster than the linear chromosomes, but their durations do not differ much (the average deviation is in all cases less than 15%).

### Appendix C: Determination of the parameters $\alpha$ , $\beta$ and $t_0$ in the formula for the distribution of $T_i$

Eq. 3 in the main text, describing the replication timing of one inter-origin region contains the parameters  $\alpha$ ,  $\beta$  and  $t_0$ , which need to be related to the biologically measurable parameters (inter-origin distance and origin rates). To estimate such parameters for the distribution of  $T_i$  we used two methods. The first is a fit of all the  $T_i$  data taken from the simulation of the given chromosome, and the second is to fit the specific  $T_i$  data (replication times of the central inter-origin region) extracted from simulation of a linear chromosomal fragment where inter-origin distances and origin strengths are sampled from known distributions (different samples for different runs of the simulation). In this second method, each run of the simulation is carried out considering inter-origin distances and origin strengths with the same averages as the original chromosome. Both methods give the same distribution for  $T_i$ , which agrees very well with Eq. 3 of the main text (See Fig. S3).

We mainly used the second method since it does not depend on origin configuration of the original chromosome. The detailed procedure is the following. First, we defined a characteristic distance  $d_c = (\frac{\gamma+1}{\lambda}) \log(\frac{1}{1-x})^{\frac{1}{1+\gamma}} v$ , where  $x < 1$  (e.g. 0.99) and as-

sume  $n_c = \min(\lfloor d_c/\langle d \rangle \rfloor + 1, \lfloor n/2 \rfloor) + 1$ . Then we produced a linear chromosomal fragment with  $2n_c$  origins, in which two origins are always located at the ends. Next, we simulated many realizations for the replication of this chromosome. In each simulation run, we sampled inter-origin distance  $d_i$ , origin strength  $\lambda_j$  and origin firing time  $t_f^{(j)}$  from  $\Gamma(\frac{\langle d \rangle^2}{\sigma^2(d)}, \frac{\langle d \rangle}{\sigma^2(d)})$ ,  $\Gamma(\frac{\langle \lambda \rangle^2}{\sigma^2(\lambda)}, \frac{\langle \lambda \rangle}{\sigma^2(\lambda)})$  and  $f(t) = \lambda_i t^\gamma \theta(t) \exp(-\lambda_i \frac{t^{\gamma+1}}{\gamma+1})$  respectively, where  $i \in \{1, 2, \dots, 2n_c - 1\}$  and  $j \in \{1, 2, \dots, 2n_c\}$ . The statistics over different realizations gives the distribution of the replication time of the central inter-origin region ( $T_{n_c}$ ), which was fitted with Eq. S1 to obtain  $\alpha$ ,  $\beta$  and  $t_0$ .

#### Appendix D: Analytical derivation of an approximate distribution of S-phase duration $T_S$ based on extreme value theory.

This section gives further details on the analytical calculation for the extreme-value estimate of the distribution of S-phase duration. We assume that replication timing of one inter-origin region  $T_i$  obeys the stretched exponential distribution

$$F(t) = P(T_i < t) = 1 - e^{-\alpha(t-t_0)^\beta}, \quad (\text{S1})$$

where  $t \geq t_0$  and  $\alpha > 0$ . The parameters  $\alpha$ ,  $\beta$  and  $t_0$  were obtained as described in the previous section. We define  $M_n = \max(T_1, T_2, \dots, T_n)$ . By taking  $a_n = 1/(\alpha^{1/\beta} \beta (\log n)^{1-1/\beta})$  and  $b_n = (\log n/\alpha)^{1/\beta} + t_0$ , and applying the Fisher-Tippett-Gnedenko theorem, we can prove that

$$\lim_{n \rightarrow \infty} P((M_n - b_n)/a_n \leq t) = \exp(-\exp(-t)) \triangleq G(t), \quad (\text{S2})$$

where  $G(t)$  is the standard Gumbel distribution.

When  $n$  is sufficiently large, we can make the approximation  $P((M_n - b_n)/a_n \leq t) \approx G(t)$ . If we define  $\tilde{t} = a_n t + b_n$ , we have  $P(M_n \leq \tilde{t}) \approx G((\tilde{t} - b_n)/a_n)$ .

Finally, we can represent the distribution of  $T_S (=M_n)$  approximately as

$$\begin{aligned} P(T_S \leq t) &\approx \exp(-\exp(-\frac{t-b_n}{a_n})) \\ &= \exp\left\{-\exp\left[\beta \log n \left(1 - (\alpha/\log n)^{1/\beta}(t-t_0)\right)\right]\right\} \end{aligned} \quad (\text{S3})$$

Here  $n$  is the origin number, and  $\alpha$ ,  $\beta$  and  $t_0$  are connected to the model parameters describing replication

kinetics,  $v$ ,  $\gamma$ , inter-origin distances ( $d_1, d_2, \dots, d_n$ ) and origin strengths ( $\lambda_1, \lambda_2, \dots, \lambda_n$ ).

We now discuss how  $\alpha$ ,  $\beta$  and  $t_0$  can be expressed as functions of simplified parameters by numerically solving some approximate equations. We consider a ‘‘characteristic’’ inter-origin region with the distance  $\langle d \rangle$  and origin strength  $\langle \lambda \rangle$ , and we assume that the replication of the inter-origin region is mainly carried out by the forks originated from the two nearest origins, both of which are typically activated. Thus we have

$$T_i \approx \langle d \rangle / 2v + (t_f^l + t_f^r)/2, \quad (\text{S4})$$

where  $t_f^l$  and  $t_f^r$  are the firing time of the left origin and the right origin respectively. Since  $t_0$  is the minimal replication time of inter-origin region and the firing time has zero as a lower bound, one has

$$t_0 = \min(T_i) = \langle d \rangle / 2v. \quad (\text{S5})$$

From equation S4, we can further obtain

$$\langle T_i \rangle \approx \langle d \rangle / 2v + \langle t_f \rangle \quad (\text{S6})$$

and

$$\sigma(T_i) \approx \sigma(t_f) \quad (\text{S7})$$

In addition, we have

$$\langle T_i \rangle = \alpha^{-\frac{1}{\beta}} \Gamma\left(\frac{1}{\beta} + 1\right) + t_0, \quad (\text{S8})$$

$$\sigma(T_i) = \alpha^{-\frac{2}{\beta}} \left[ \Gamma\left(\frac{2}{\beta} + 1\right) - \Gamma^2\left(\frac{1}{\beta} + 1\right) \right], \quad (\text{S9})$$

$$\langle t_f \rangle = \left(\frac{\gamma+1}{\langle \lambda \rangle}\right)^{\frac{1}{\gamma+1}} \Gamma\left(\frac{\gamma+2}{\gamma+1}\right), \quad (\text{S10})$$

and

$$\sigma(t_f) = \left(\frac{\gamma+1}{\langle \lambda \rangle}\right)^{\frac{1}{\gamma+1}} \sqrt{\Gamma\left(\frac{\gamma+3}{\gamma+1}\right) - \Gamma^2\left(\frac{\gamma+2}{\gamma+1}\right)} \quad (\text{S11})$$

Based on equations S5-S11,  $\alpha$  and  $\beta$  can be numerically solved as functions of  $v$ ,  $\gamma$ ,  $\langle d \rangle$  and  $\langle \lambda \rangle$ . Our simulations in the EVD regime, and using empirically realistic values of the parameters are in line with equations S5-S7.

- 
- [1] A. C. Leonard and M. Méchali, Cold Spring Harbor perspectives in biology **5**, a010116 (2013).  
 [2] D. M. Gilbert, Science **294**, 96 (2001).  
 [3] J. Bechhoefer and N. Rhind, Trends in Genetics **28**, 374 (2012).

- [4] S. P. Das, T. Borrmann, V. W. T. Liu, S. C.-H. Yang, J. Bechhoefer, and N. Rhind, Genome Res **25**, 1886 (2015).  
 [5] S. C.-H. Yang, N. Rhind, and J. Bechhoefer, Molecular systems biology **6**, 404 (2010).

- [6] M. Hawkins, R. Retkute, C. A. Müller, N. Saner, T. U. Tanaka, A. P. de Moura, and C. A. Nieduszynski, *Cell reports* **5**, 1132 (2013).
- [7] N. Agier, O. M. Romano, F. Touzain, M. Cosentino Lagomarsino, and G. Fischer, *Genome biology and evolution* **5**, 370 (2013).
- [8] R. Retkute, C. A. Nieduszynski, and A. de Moura, *Physical Review E* **86**, 031916 (2012).
- [9] A. Baker, B. Audit, S. C.-H. Yang, J. Bechhoefer, and A. Arneodo, *Phys Rev Lett* **108**, 268101 (2012).
- [10] A. Gispan, M. Carmi, and N. Barkai, *Genome research* (2016), 10.1101/gr.205849.116.
- [11] R. E. Boulos, G. Drillon, F. Argoul, A. Arneodo, and B. Audit, *FEBS Lett* **589**, 2944 (2015).
- [12] B. Moindrot, B. Audit, P. Klous, A. Baker, C. Thermes, W. de Laat, P. Bouvet, F. Mongelard, and A. Arneodo, *Nucleic Acids Res* **40**, 9470 (2012).
- [13] B. D. Pope, T. Ryba, V. Dileep, F. Yue, W. Wu, O. Denas, D. L. Vera, Y. Wang, R. S. Hansen, T. K. Canfield, *et al.*, *Nature* **515**, 402 (2014).
- [14] J. N. Bianco, J. Poli, J. Saksouk, J. Bacal, M. J. Silva, K. Yoshida, Y.-L. Lin, H. Tourrière, A. Lengronne, and P. Pasero, *Methods* **57**, 149 (2012).
- [15] S. C.-H. Yang and J. Bechhoefer, *Physical Review E* **78**, 041917 (2008).
- [16] J. Bechhoefer and B. Marshall, *Physical review letters* **98**, 098105 (2007).
- [17] H. Masai, S. Matsumoto, Z. You, N. Yoshizawa-Sugata, and M. Oda, *Annual review of biochemistry* **79**, 89 (2010).
- [18] M. Méchali, K. Yoshida, P. Coulombe, and P. Pasero, *Current opinion in genetics & development* **23**, 124 (2013).
- [19] J. Herrick, S. Jun, J. Bechhoefer, and A. Bensimon, *Journal of molecular biology* **320**, 741 (2002).
- [20] A. P. de Moura, R. Retkute, M. Hawkins, and C. A. Nieduszynski, *Nucleic acids research* , gkq343 (2010).
- [21] E. Z. Meilikhov and R. M. Farzetzdinova, *JETP Letters* **102**, 55 (2015).
- [22] C. Heichinger, C. J. Penkett, J. Bähler, and P. Nurse, *The EMBO Journal* **25**, 5171 (2006).
- [23] B. V. Gnedenko and A. N. Kolmogorov, *Limit distributions for sums of independent random variables* (Addison-Wesley, Cambridge, MA, 1954).
- [24] V. M. Zolotarev, *One-dimensional stable distributions* (American Mathematical Society, 1986).
- [25] J. A. Vincent, T. J. Kwong, and T. Tsukiyama, *Nature structural & molecular biology* **15**, 477 (2008).
- [26] A. S. Kennard, M. Osella, A. Javer, J. Grilli, P. Nghe, S. J. Tans, P. Cicuta, and M. Cosentino Lagomarsino, *Phys Rev E* **93**, 012408 (2016).
- [27] A. Giometto, F. Altermatt, F. Carrara, A. Maritan, and A. Rinaldo, *Proc Natl Acad Sci U S A* **110**, 4646 (2013).
- [28] A. Letessier, G. A. Millot, S. Koundrioukoff, A.-M. Lachags, N. Vogt, R. S. Hansen, B. Malfoy, O. Brison, and M. Debatisse, *Nature* **470**, 120 (2011).
- [29] R. S. Cha and N. Kleckner, *Science (New York, N.Y.)* **297**, 602 (2002).
- [30] A. S. Ivessa, B. A. Lenzmeier, J. B. Bessler, L. K. Goudsouzian, S. L. Schnakenberg, and V. A. Zakian, *Molecular cell* **12**, 1525 (2003).
- [31] D. Fachinetti, R. Bermejo, A. Cocito, S. Minardi, Y. Kato, Y. Kanoh, K. Shirahige, A. Azvolinsky, V. A. Zakian, and M. Foiani, *Molecular cell* **39**, 595 (2010).
- [32] P. Pasero, A. Bensimon, and E. Schwob, *Genes & development* **16**, 2479 (2002).
- [33] R. Retkute, C. A. Nieduszynski, and A. de Moura, *Physical review letters* **107**, 068103 (2011).
- [34] M. M. Magiera, E. Gueydon, and E. Schwob, *The Journal of cell biology* **204**, 165 (2014).
- [35] K. M. Schmoller, J. J. Turner, M. Kõivomägi, and J. M. Skotheim, *Nature* **526**, 268 (2015).
- [36] J. M. Skotheim, *Mol Biol Cell* **24**, 678 (2013).
- [37] A. T. Hahn, J. T. Jones, and T. Meyer, *Cell cycle (Georgetown, Tex.)* **8**, 1044 (2009).
- [38] B. T. Bajar, A. J. Lam, R. K. Badiie, Y.-H. Oh, J. Chu, X. X. Zhou, N. Kim, B. B. Kim, M. Chung, A. L. Yablonovitch, B. F. Cruz, K. Kullalart, J. J. Tao, T. Meyer, X.-D. Su, and M. Z. Lin, *Nature methods* **13**, 993 (2016).
- [39] A. Adiciptaningrum, M. Osella, M. C. Moolman, M. Cosentino Lagomarsino, and S. J. Tans, *Sci Rep* **5**, 18261 (2015).
- [40] A. Koren, I. Soifer, and N. Barkai, *Genome research* **20**, 781 (2010).
- [41] A. Gispan, M. Carmi, and N. Barkai, *BMC biology* **12**, 79 (2014).
- [42] J. Karschau, J. J. Blow, and A. P. de Moura, *Physical review letters* **108**, 058101 (2012).
- [43] D. M. Czajkowsky, J. Liu, J. L. Hamlin, and Z. Shao, *Journal of molecular biology* **375**, 12 (2008).
- [44] R. Fraser and P. Nurse, *Journal of cell science* **35**, 25 (1979).
- [45] M. Imakaev, G. Fudenberg, R. P. McCord, N. Naumova, A. Goloborodko, B. R. Lajoie, J. Dekker, and L. A. Mirny, *Nature methods* **9**, 999 (2012).
- [46] H. Mahbubani, T. Paull, J. Elder, and J. Blow, *Nucleic acids research* **20**, 1457 (1992).
- [47] K. Nasmyth and P. Nurse, *Journal of cell science* **39**, 215 (1979).
- [48] T. Ryba, I. Hiratani, J. Lu, M. Itoh, M. Kulik, J. Zhang, T. C. Schulz, A. J. Robins, S. Dalton, and D. M. Gilbert, *Genome research* **20**, 761 (2010).
- [49] M. Vanoni, M. Vai, L. Popolo, and L. Alberghina, *Journal of bacteriology* **156**, 1282 (1983).
- [50] X. Yang, K.-Y. Lau, V. Sevim, and C. Tang, *PLoS Biol* **11**, e1001673 (2013).

## SUPPLEMENTARY FIGURES AND TABLES

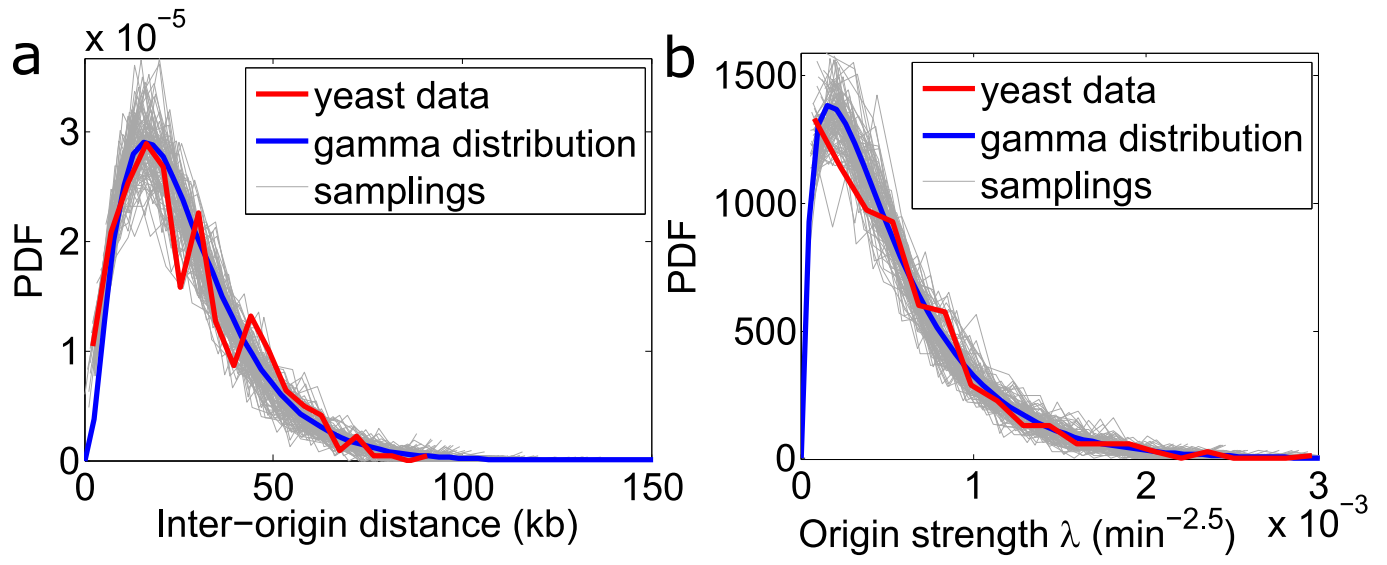


FIG. S1. The hypothesis of gamma-distributed inter-origin distances and origin firing rates used to generate randomized chromosomes is in line with empirical data. The plots compare inter-origin distances (a) and firing rates (b) distributions used for the model (blue continuous line) with *S. cerevisiae* data from ref. [6] (red line), and 100 samplings of the assumed distributions with the same number of instances as the empirical case (thin grey lines). Empirical firing rates were inferred setting  $\gamma = 1.5$  (the best-fit value for the data in ref. [6]).

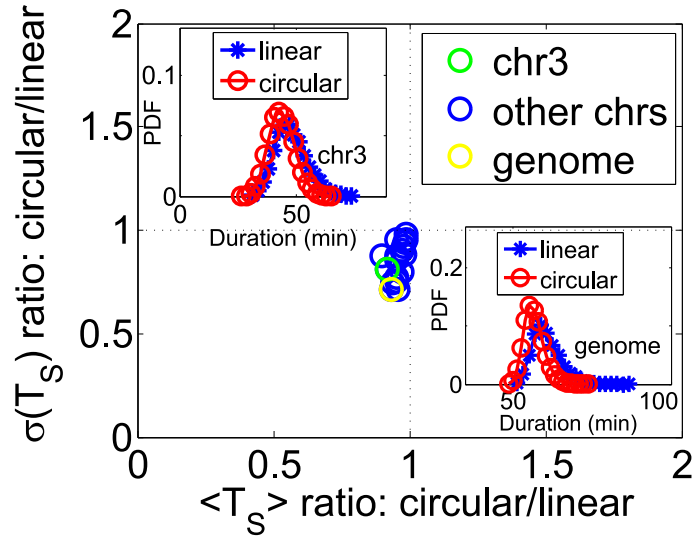


FIG. S2. Comparison of S-phase duration of *S.cerevisiae* chromosomes and genome and their circularized versions indicates that the boundary effect on replication timing is small. Circular chromosomes were obtained by linking two ends of the linear chromosome. The circular genome was gotten by linking all the linear chromosomes via their ends successively. Ratio of  $T_S$  average (SD) between *S.cerevisiae* linear chromosomes and the genome and the circularized versions is close to 1. The insets show that the distribution of  $T_S$  of chromosome 3 and the genome and their circularized versions are similar. The parameters giving best fit to *S. cerevisiae* data from ref. [6] were used (in particular,  $\gamma = 1.5$ ).

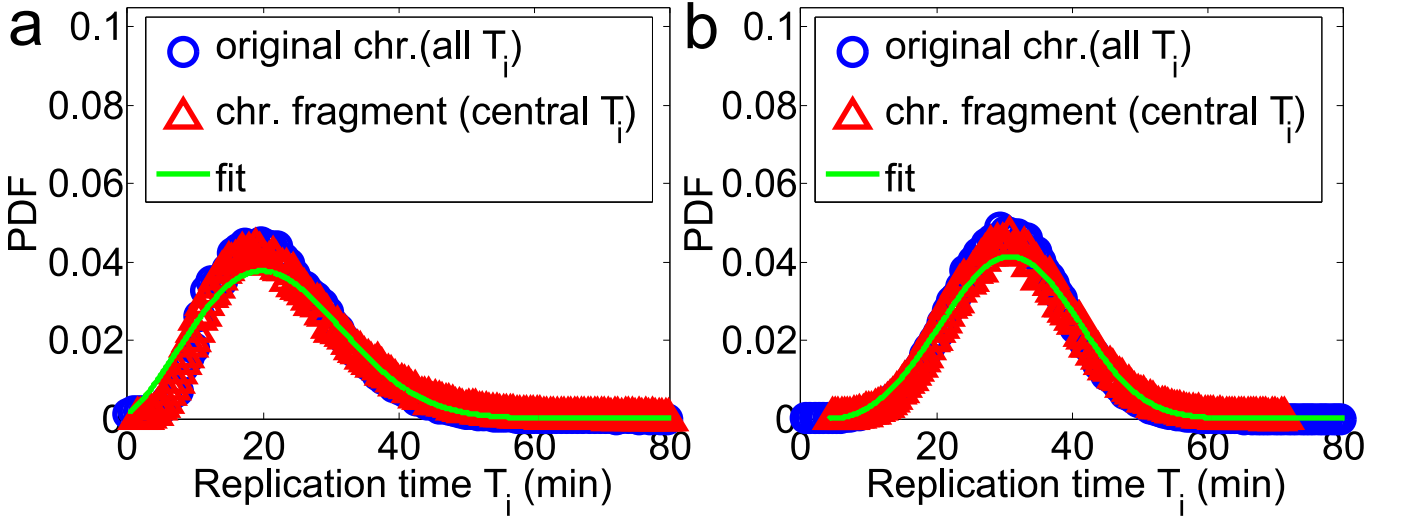


FIG. S3. **Justification of the assumption for the inter-origin replication timing distribution (Eq. 3 of the main text).** We used two methods of obtaining the data for the distribution of replication time ( $T_i$ ) of inter-origin regions, both of which are in good agreement with the theoretical formula. Blue circles: distribution obtained by the simulation of a circular chromosome (original chromosome) where origin strengths and inter-origin distances are sampled with Eq.2; red triangles: distribution of replication time of the central inter-origin region in a linear chromosomal fragment where origin strengths and inter-origin distances are sampled with Eq.2 in each run of the simulation; the continuous line is a fit with Eq. 3. For (a), chromosome parameters:  $\gamma = 0$ ,  $n = 20$  (original) or 16 (linear fragment),  $v = 1.88 \text{ kb/min}$ ,  $\langle d \rangle = 28.13 \text{ kb}$ ,  $\sigma(d) = 13.46 \text{ kb}$ ,  $\langle \lambda \rangle = 0.045 \text{ min}^{-1}$ ,  $\sigma(\lambda) = 0.036 \text{ min}^{-1}$ , and the fitted parameters:  $\alpha = 3.72 \times 10^{-4} \text{ min}^{-\beta}$ ,  $\beta = 2.42$ ,  $t_0 = -1.07 \text{ min}$ . For (b), chromosome parameters:  $\gamma = 1.5$  (best fit),  $n = 20$  (original) or 10 (linear fragment),  $v = 1.81 \text{ kb/min}$ ,  $\langle d \rangle = 28.13 \text{ kb}$ ,  $\sigma(d) = 13.46 \text{ kb}$ ,  $\langle \lambda \rangle = 6.17 \times 10^{-4} \text{ min}^{-2.5}$ ,  $\sigma(\lambda) = 5.53 \times 10^{-4} \text{ min}^{-2.5}$ , and the fitted parameters:  $\alpha = 1.79 \times 10^{-5} \text{ min}^{-\beta}$ ,  $\beta = 3.21$ ,  $t_0 = 4.16 \text{ min}$ .

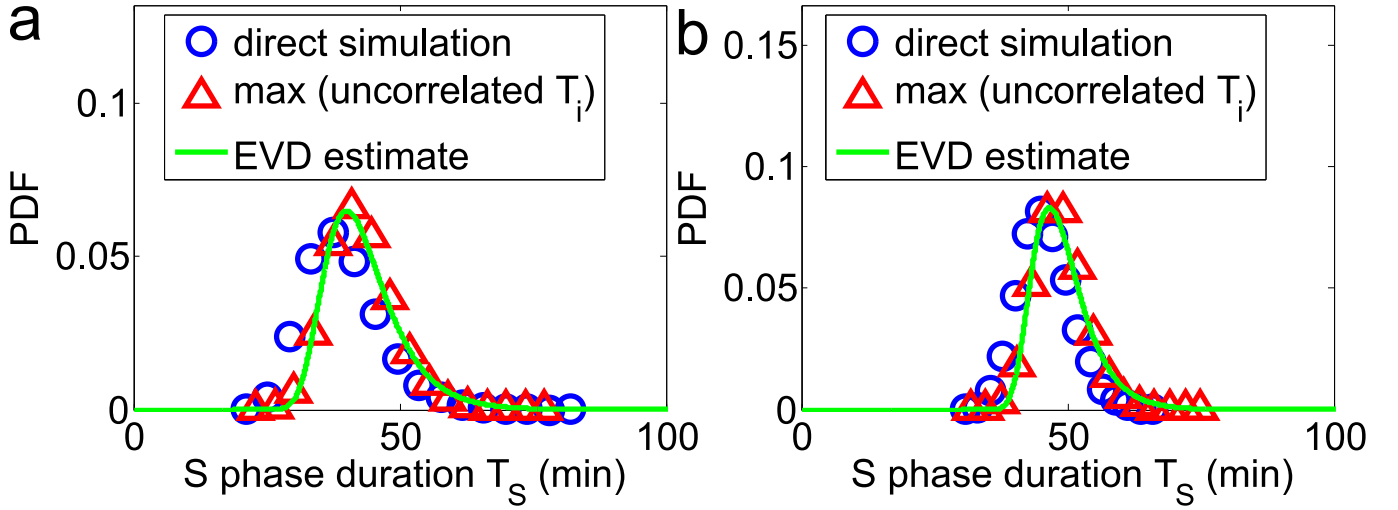


FIG. S4. **The correlation between replication times of adjacent inter-origin regions has little effect on the distribution of S-phase duration  $T_S$ .** The plot shows the distribution of S-phase duration from direct simulation (blue circles; correlated  $T_i$ ) compared to sampling of  $T_i (i \in \{1, 2, \dots, n\})$  from  $F(t) = 1 - e^{-\alpha(t-t_0)^\beta}$  independently and taking their maximum (red triangles; uncorrelated  $T_i$ ). Both methods agree well with the EVD estimate based on Eq. 4 of the main text (green continuous line). The plots refers to a circular chromosome with two different parameter sets, compatible with yeast data: (a)  $\gamma = 0$ ,  $n = 20$ ,  $v = 1.88 \text{ kb/min}$ ,  $\langle d \rangle = 28.13 \text{ kb}$ ,  $\sigma(d) = 13.46 \text{ kb}$ ,  $\langle \lambda \rangle = 0.045 \text{ min}^{-1}$ ,  $\sigma(\lambda) = 0.036 \text{ min}^{-1}$ , (b)  $\gamma = 1.5$ ,  $n = 20$ ,  $v = 1.81 \text{ kb/min}$ ,  $\langle d \rangle = 28.13 \text{ kb}$ ,  $\sigma(d) = 13.46 \text{ kb}$ ,  $\langle \lambda \rangle = 6.17 \times 10^{-4} \text{ min}^{-2.5}$ ,  $\sigma(\lambda) = 5.53 \times 10^{-4} \text{ min}^{-2.5}$ . Origin strengths and inter-origin distances are sampled with Eq. 2 of the main text.

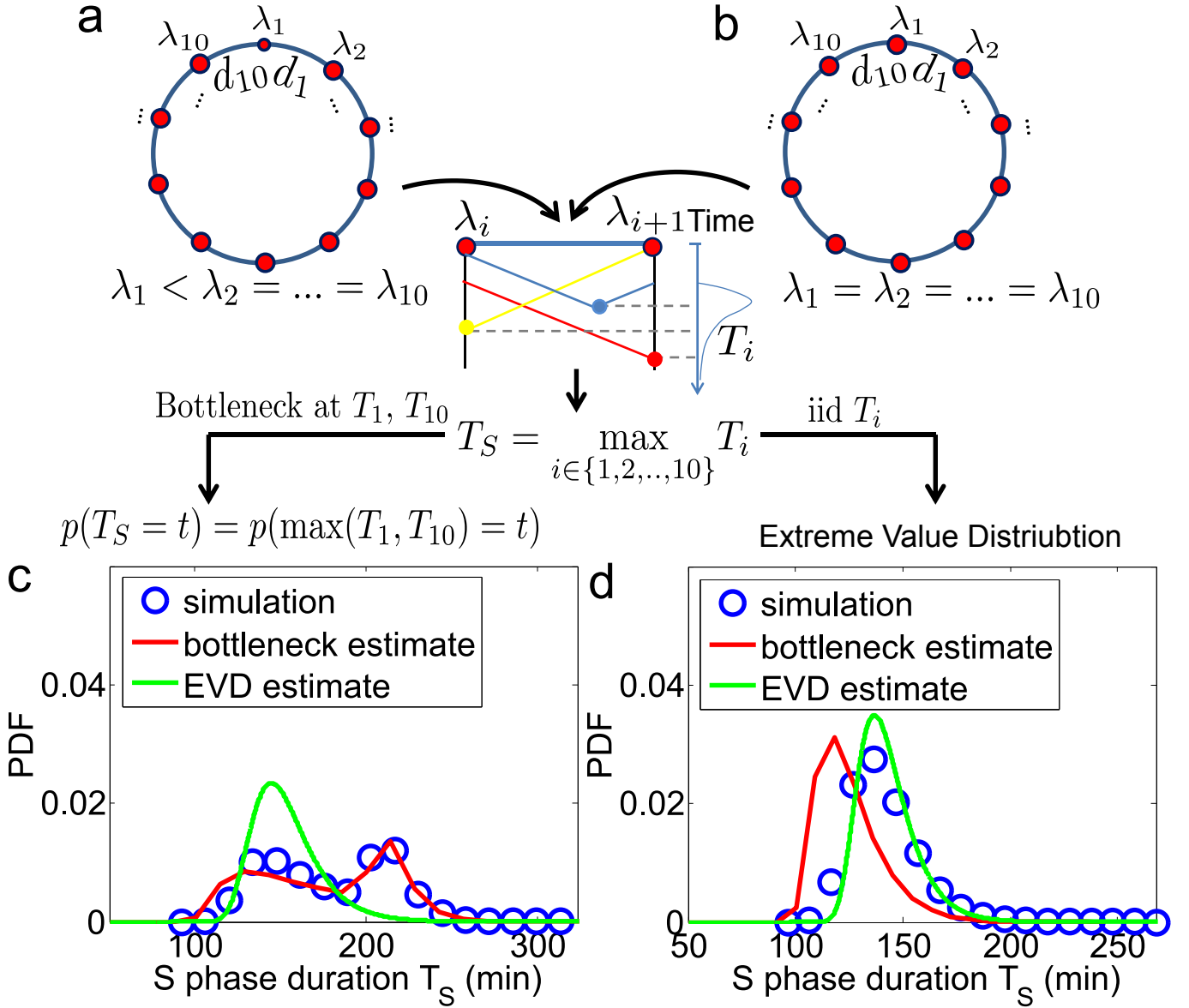


FIG. S5. **Replication regimes determined by firing rates.** (a) Due to a single slow-firing origin, the two neighboring bottleneck inter-origin regions (labelled by the index 10 and 1 in panels a and b) typically complete replication much later than the rest. Hence,  $T_S$  will be typically equal to  $\max(T_1, T_{10})$  (origin strengths in the example are  $\lambda_i = 0.055 \text{ min}^{-1}$  for all origins except  $\lambda_1 = 0.0055 \text{ min}^{-1}$ ). (b) If the replication times of all inter-origin regions are comparable, and they are considered independent and identically-distributed (iid) random variables, the distribution of  $T_S$  can be obtained by extreme-value-distribution (EVD) theory (origin strengths are  $\lambda_i = 0.05 \text{ min}^{-1}$ ). Simulations of the model (blue circles), when one inter-origin distance is much larger than the others (c), and when all inter-origin distances and strengths are comparable (d), agree with the corresponding analytical calculations (red and green curves). (Origin number  $n = 10$  origins, fork velocity  $v = 1 \text{ kb/min}$ , origin strength  $d_i = 200 \text{ kb}$ .)



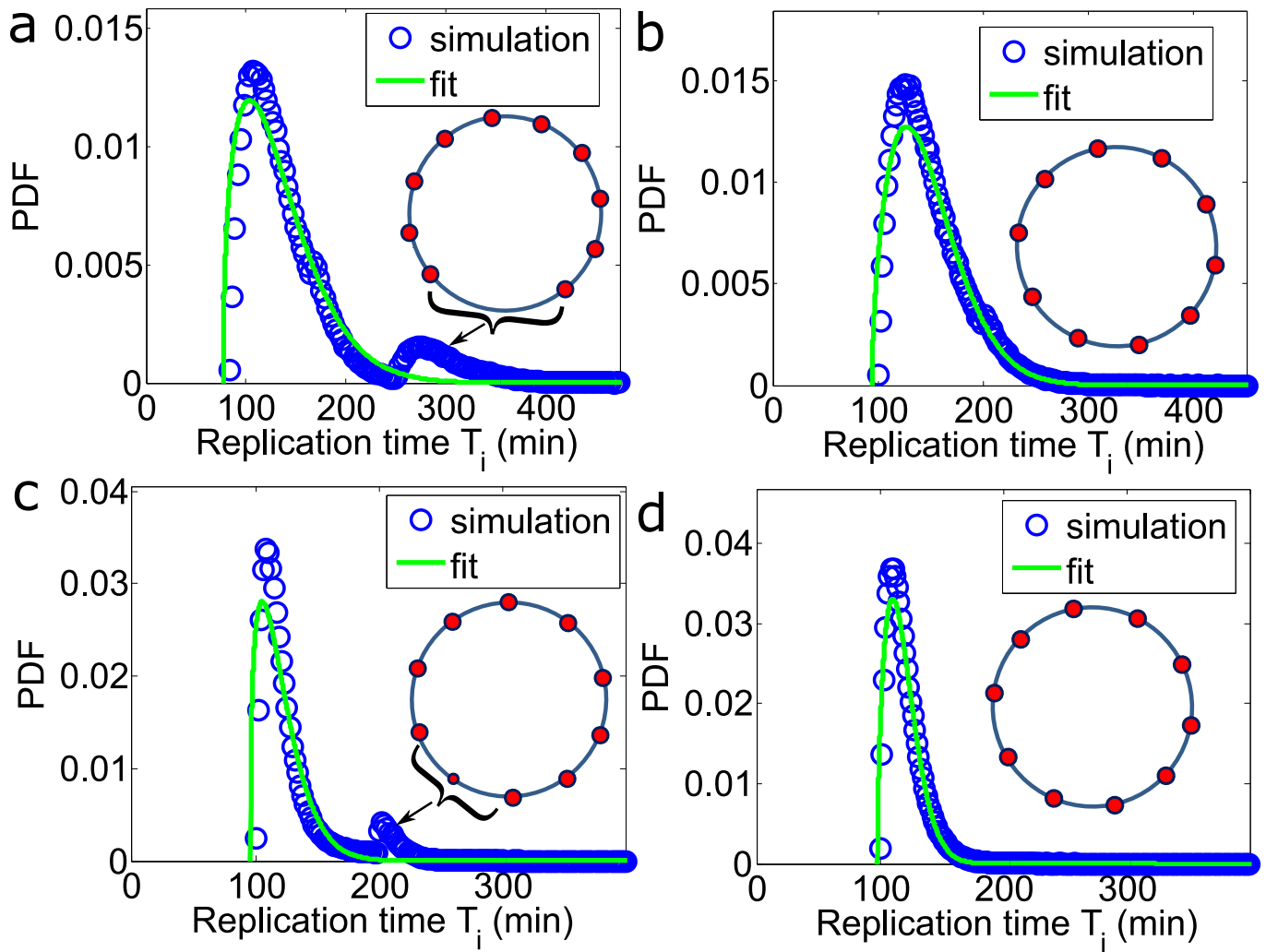


FIG. S6. In the bottleneck regime, the slowest region in replication causes the appearance of small peaks in the right tail of the distribution of  $T_i$ , leading to the failure of the EVD estimate. The plots come from simulations with parameter sets shown in Fig. S5 and in Fig. 2 of the main text. For the bottleneck cases shown in Fig. 2 of the main text (a) and Figure S5 (c), a small peak emerges in the right tail of  $T_i$  distribution due to the slowest replication of the bottleneck regions. Conversely, in the EVD regime, the right peak does not exist (b,d).

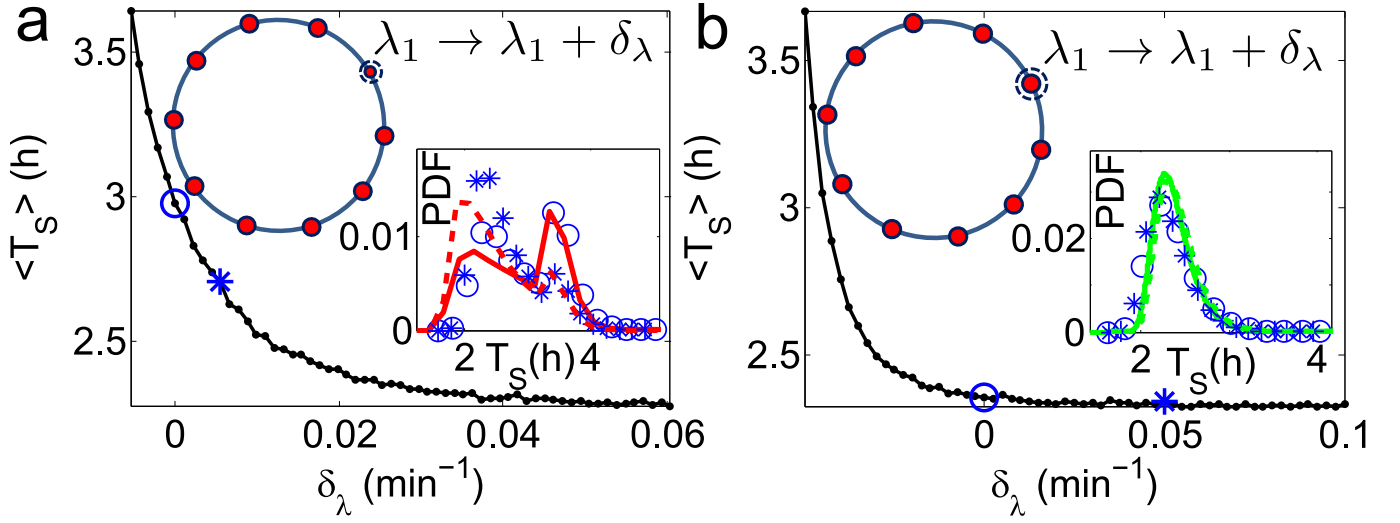


FIG. S7. **Effects of perturbations of a pair of inter-origin regions on S-phase duration.** (a) The bottleneck regions of the chromosome shown in Fig. S5a are perturbed by increasing the strength of origin 1 by  $\delta_\lambda$  (i.e.,  $\lambda_1 \rightarrow \lambda_1 + \delta_\lambda$ ). The inset shows that the perturbation changes the distribution of  $T_S$  (circles are simulations for the unperturbed chromosome, and stars correspond to  $\delta_\lambda = \lambda_1$ ; the two curves are the analytical estimates in the bottleneck regime). (b) The same perturbation as in (a) is performed on the strength of one origin of the chromosome shown in Fig. S5b, which lies in the EVD regime. Symbols are as in (a). The distribution of  $T_S$  is robust to this perturbation.

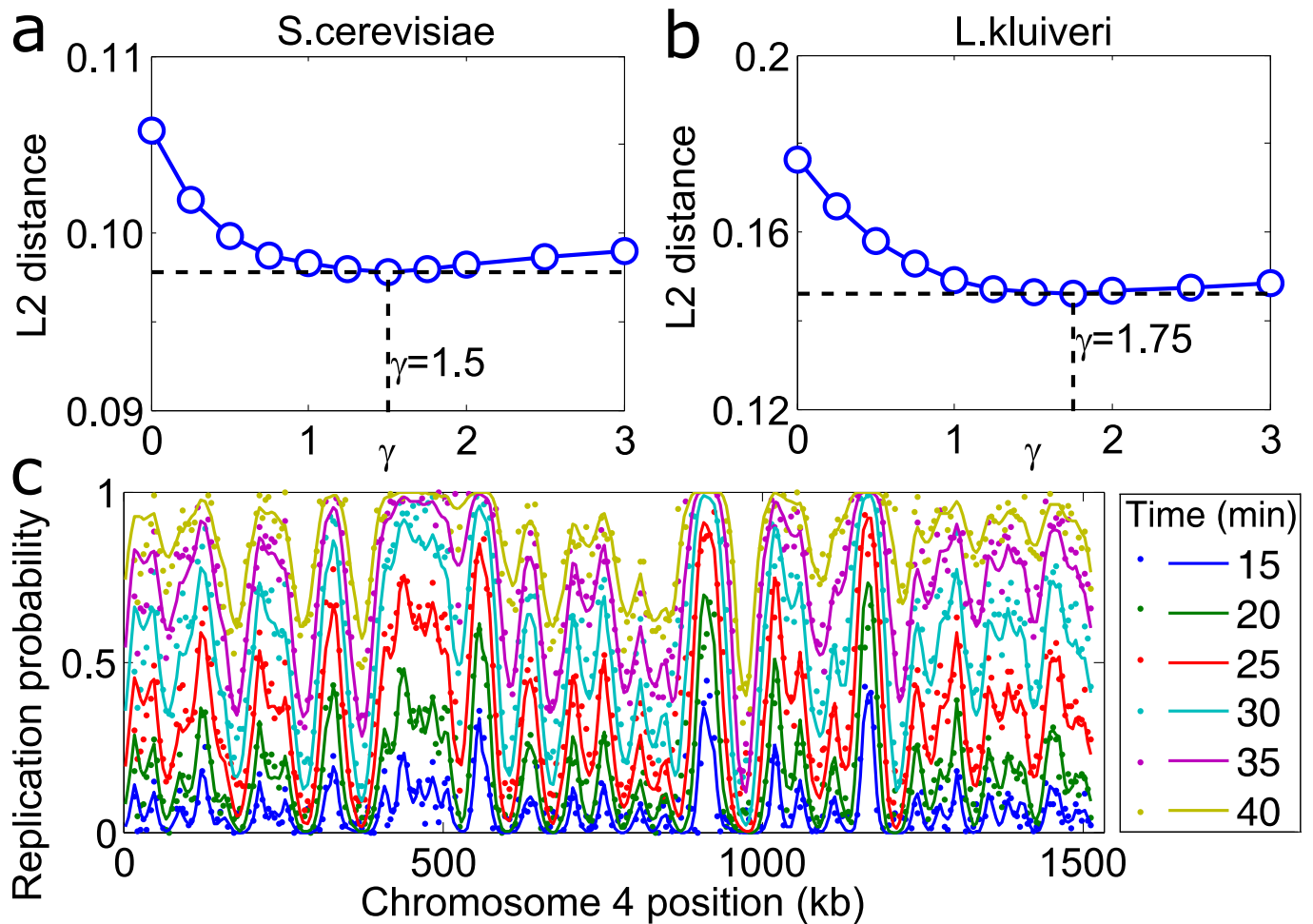


FIG. S8. The goodness of the fit of the model with the empirical data depends on exponent factor  $\gamma$  and with the best  $\gamma$ , the model can be efficiently fit to the empirical replication data. The empirical data of *L. kluyveri* and *S. cerevisiae* are from ref. [6, 7]. (a,b) The L2 distance between theoretical and empirical replication probability profiles is minimized at  $\gamma = 1.5$  (for *S. cerevisiae*) or  $\gamma = 1.75$  (for *L. kluyveri*) (c) The model gives a good fit to the empirical replication probability  $\phi(x, t)$  from *S. cerevisiae* chromosome 4. Dots and continuous lines indicate experimental and theoretical data respectively, which are both averaged with bins of 5kb. Different colors indicate different measurement times.

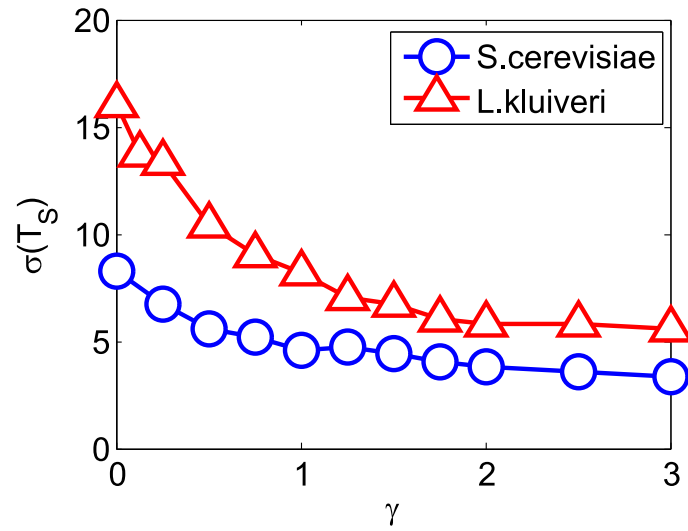


FIG. S9. **The standard deviation of S-phase duration  $T_S$  of *S. cerevisiae* and *L.kluiveri* decreases with the parameter  $\gamma$ .** The plot is obtained from simulations with the best-fitting parameters of empirical data, using data from ref. [6, 7] (See Fig. S10 and S8)

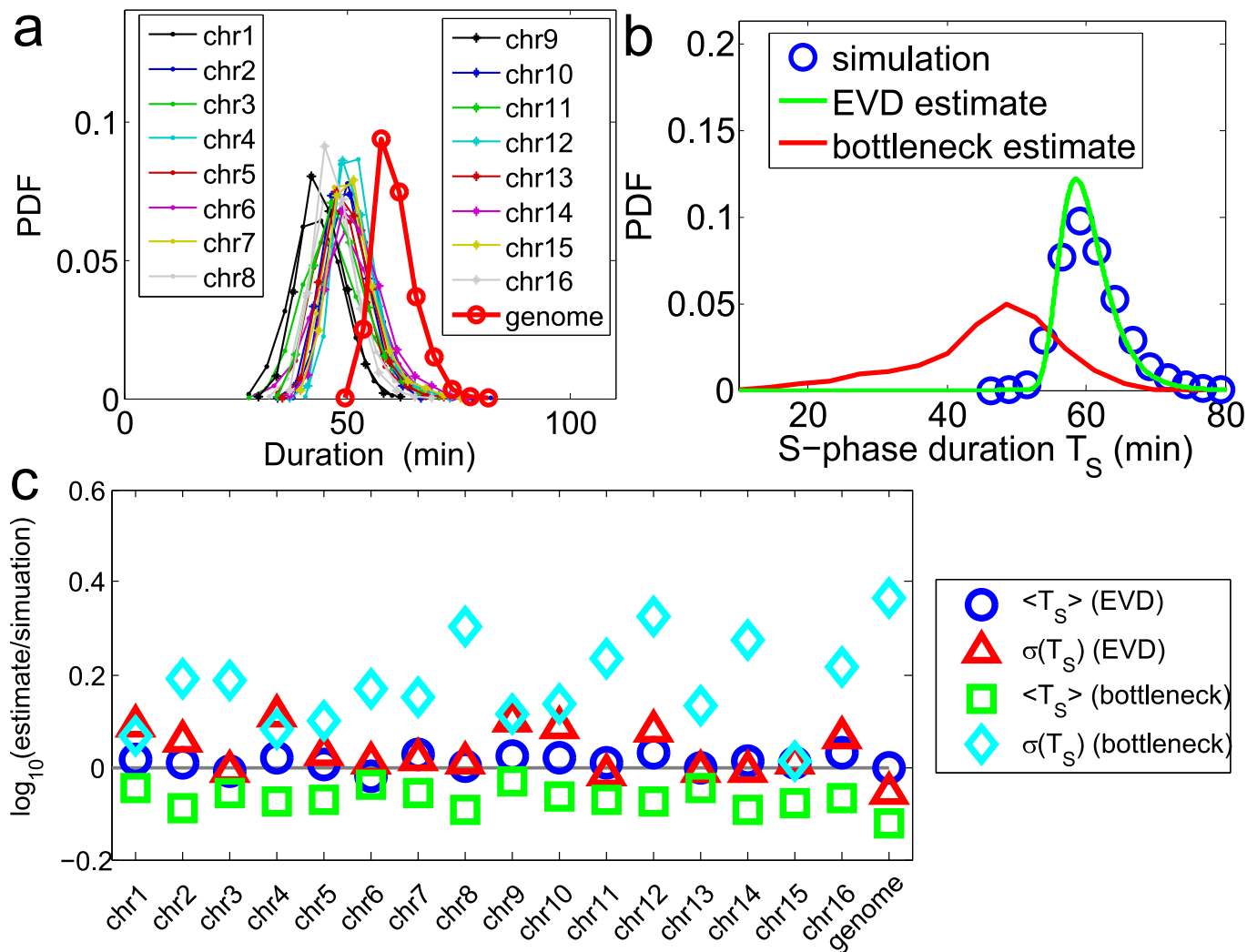


FIG. S10. Simulated and estimated prediction for the cell-to-cell variability of S-phase duration, using the best-fitting parameters for *S. cerevisiae*. (a) The plot shows the probability density function (PDF) of the predicted duration of the replication of chromosomes and genome of *S. cerevisiae* from simulations. The average duration of S phase compares well with measurements from flow cytometry [6]. (b) The simulated distribution (PDF) of the replication timing of the genome (circle), is well predicted by EVD estimate (green line) rather than the bottleneck estimate (red line). (c) Comparison of the average and standard deviation of the duration of the replication from analytical estimates and the simulation. The EVD estimate predicts the replication timing of the genome and all the chromosomes better than the bottleneck estimate. Data from ref. [6]. chr: chromosome.

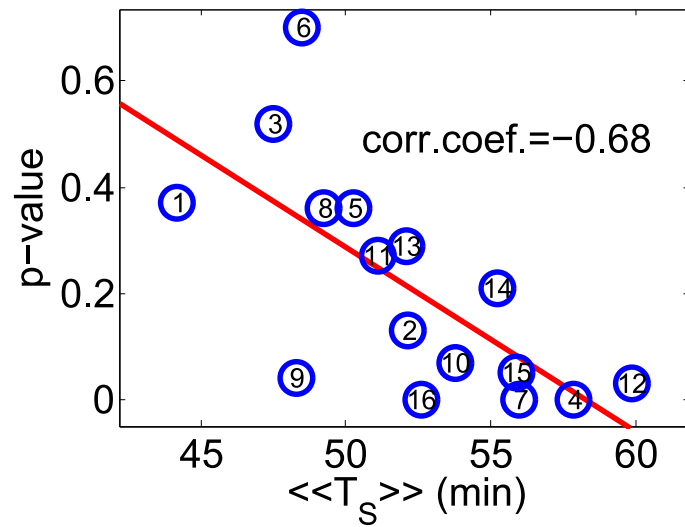


FIG. S11. **Stronger bias towards smaller replication times for slower chromosomes.** The plot shows that the p-value of the mean  $T_S$  for each *S. cerevisiae* chromosome (circles, numbered 1-16) against randomized chromosomes is negatively correlated with the typical replication timing  $T_S$  of the randomized chromosomes. See Fig. 5b of the main text. Randomized chromosomes have the same averaged inter-origin distance and averaged origin strength. The typical time in the  $x$ -axis is defined as a double mean over realizations of the parameters and over cells, i.e., realizations of the process at fixed parameters. The P-value is defined as the fraction of the mean  $T_S$  from randomized chromosomes smaller than the mean empirical  $T_S$  over the number of randomised samples.

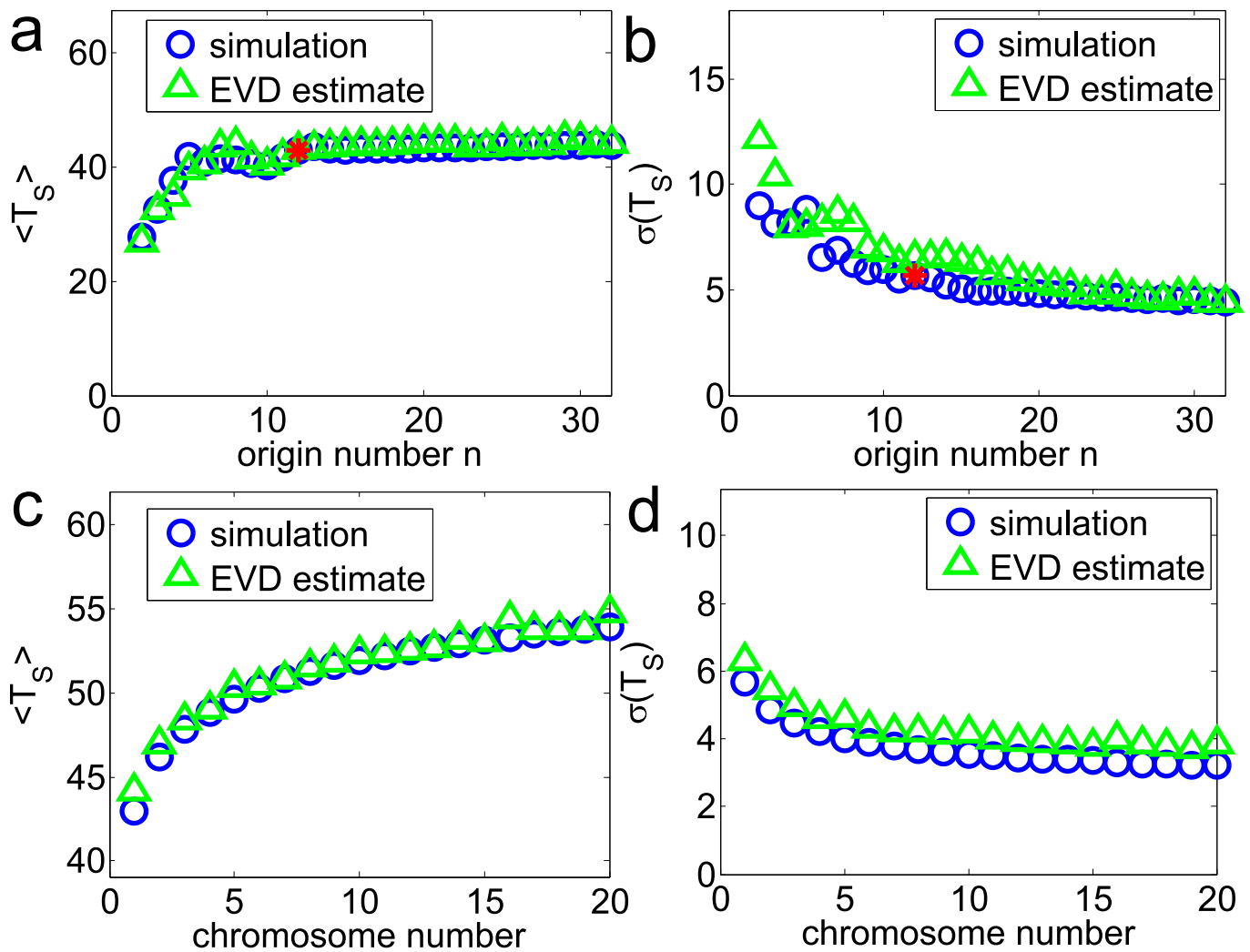


FIG. S12. Change of the overall replication timing and its cell-to-cell variability with number of inter-origin regions and with number of chromosomes. (a) Average of replication duration of *S. cerevisiae* chromosome I (parameters from the fit of data from ref. [6]) increases with origin number. The value saturates around  $n=10$ . (b) The standard deviation decreases with  $n$ . Red stars indicate the empirical value of  $n$ . (c,d) The average of the completion time for replication of *S. cerevisiae* chromosome 1 increases with the number of copies, whereas the standard deviation decreases.

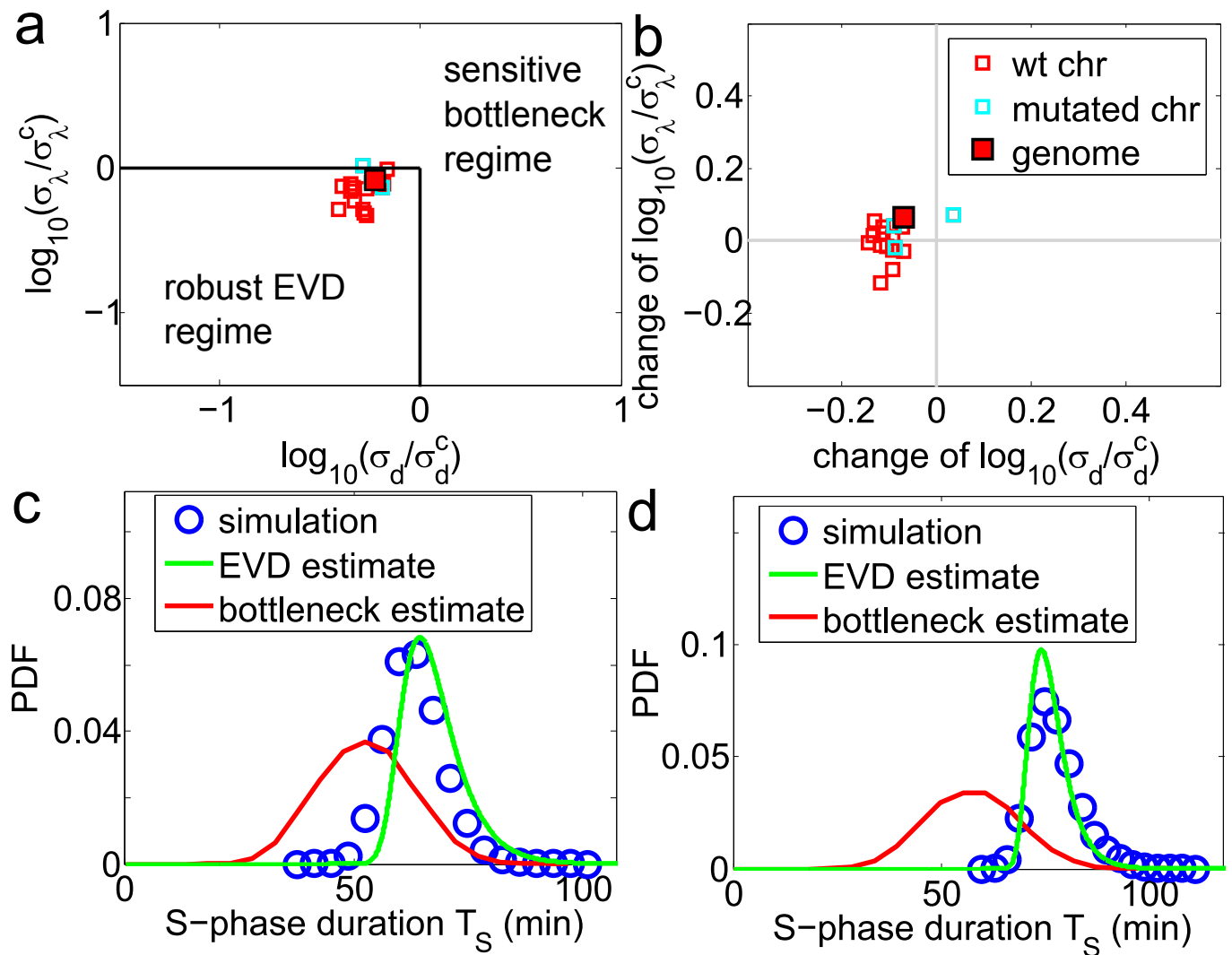


FIG. S13. *S. cerevisiae* remains in the extreme-value regime under inactivation of three origins in chromosomes **6, 7 and 10**. (a) The phase diagram indicates that all the chromosomes (except for chromosome 7) and the genome remain in the extreme-value regime when origins are removed. (b) The overall relative variability of inter-origin distances for the mutant strain does not change much compared to the wt strain. The xy-axes indicate the change of the overall relative variability of inter-origin distances ( $\log_{10}(\sigma_d/\sigma_d^c)$ ) and origin strengths ( $\log_{10}(\sigma_\lambda/\sigma_\lambda^c)$ ) of the origin mutant strain compared to the wt strain. (c,d) The extreme-value estimate predicts well the replication duration of chromosomes (e.g. chromosome 7 shown in panel c) and the genome (panel d). The plots refer to fits of data of *S. cerevisiae* origin-impaired mutant and wt strain from ref. [6].



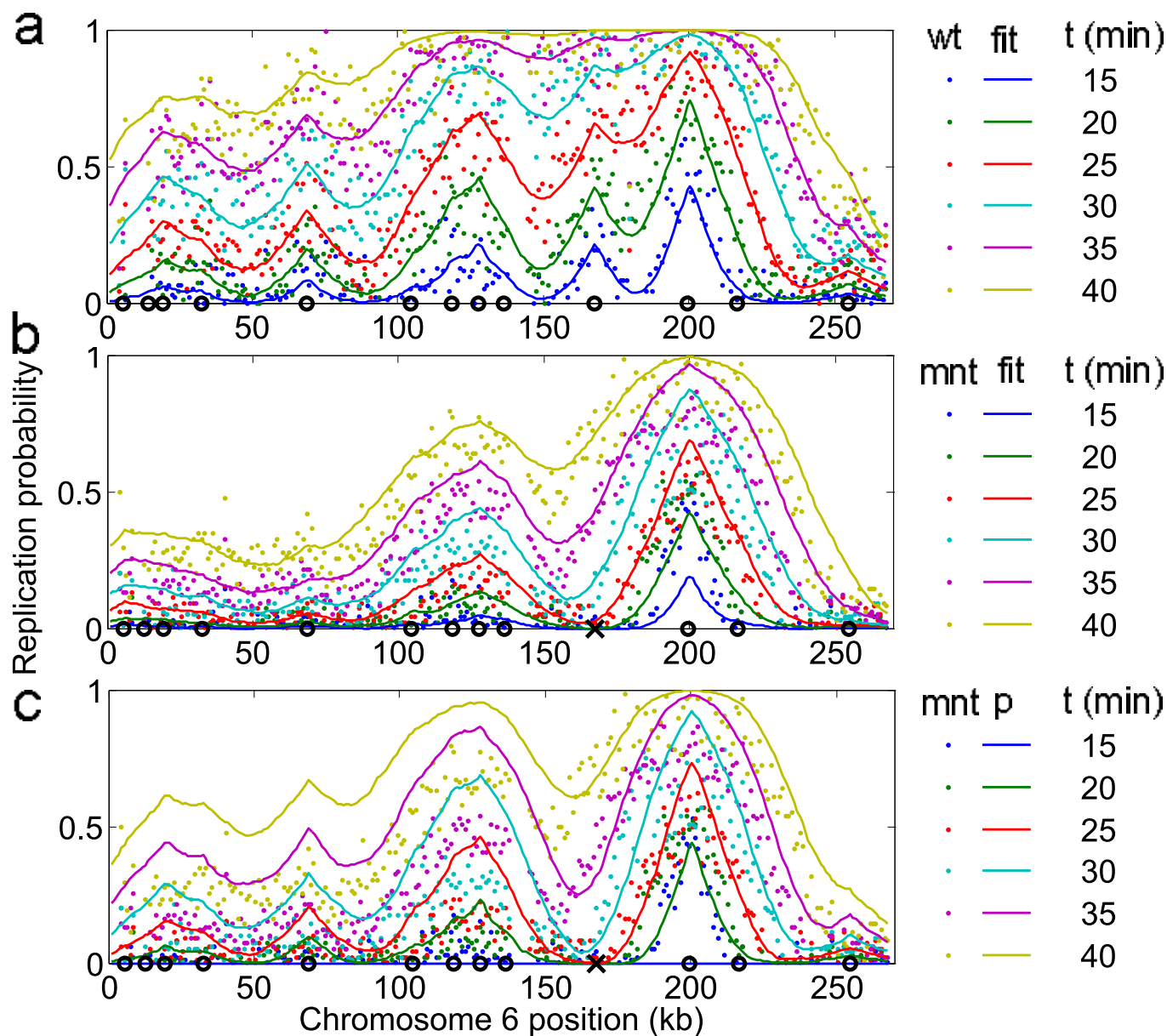


FIG. S14. The model gives a satisfactory prediction of replication timing profiles of *S. cerevisiae* origin mutant (mnt) strains. The plots refer to chromosome 6 as an example, and assess the performance of the model with parameters based on the wild-type fit on the mutant data, when simulations are run without the inactivated origins. Dots correspond to experimental data from ref. [6], and lines indicate a model fit or a model prediction (p). Different dot colors correspond to different times. The black circles indicate origin locations. The black cross mark shows the location of the inactivated origin. (a) Model fit of replication timing profiles of the wt strain. (b) Model fit of replication timing profiles of the origin mutant strain. (c) Model prediction of mutant replication timing profiles based on the best-fit parameters from the wt data.

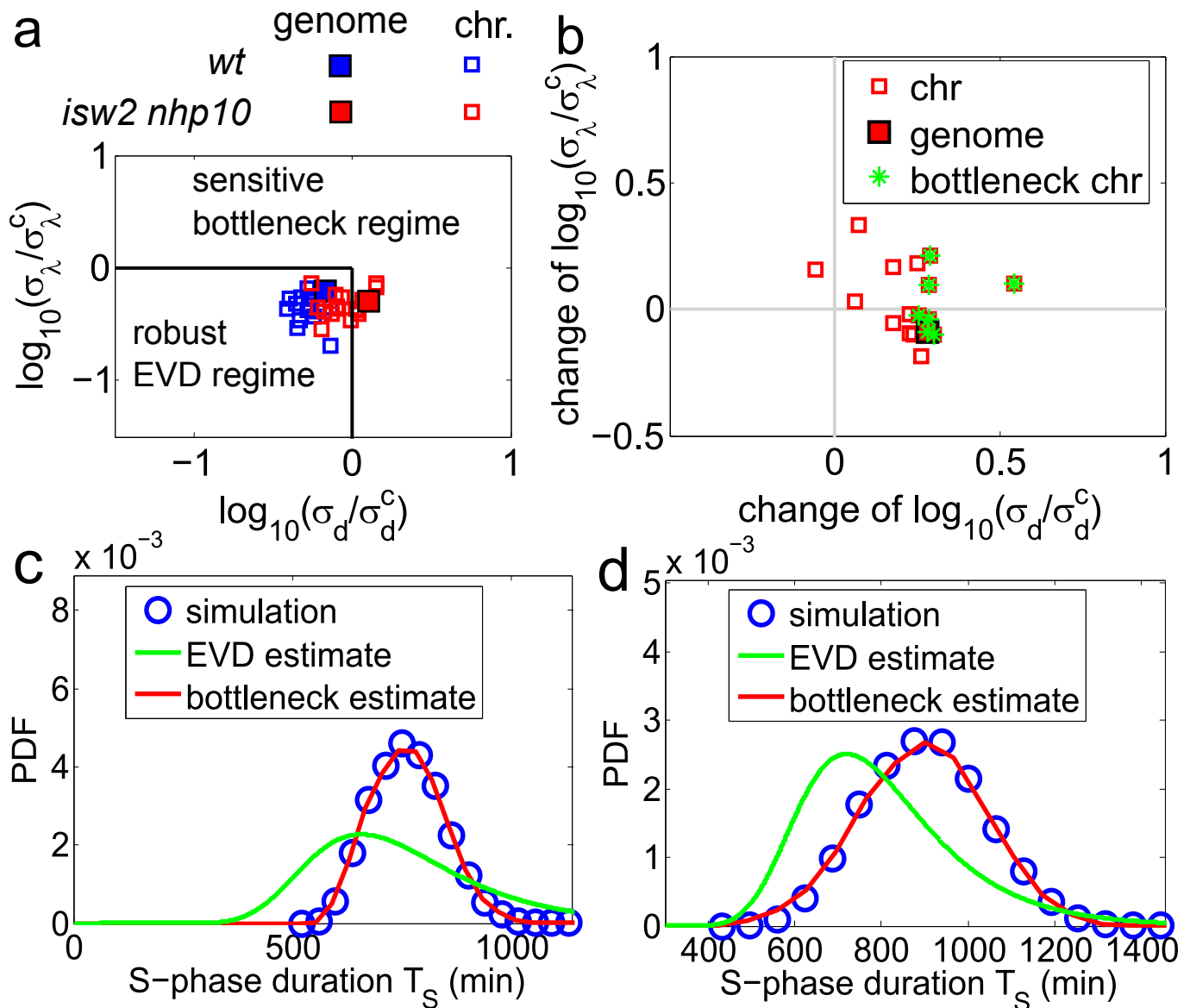


FIG. S15. *S.cerevisiae isw2/nhp10* mutant treated with DNA alkylating agent MMS (affecting replication forks) drives S-phase to the bottleneck regime. (a) The phase diagram (see Fig. 4 and 5 in the main text) indicates that all the chromosomes and the genome of the wt strain are in the EVD regime while some chromosomes (4, 6, 12, 13, 14 and 15) and the genome of the mutant are in the bottleneck regime (b) The relative variability of the inter-origin distances for the chromosomes and the genome of the mutant strain is higher than that of the wt strain (except for chromosome 1). The green stars indicate that the chromosomes/genome of the mutant strain is inside the bottleneck regime. The xy-axes indicate the change of the overall relative variability of inter-origin distances ( $\log_{10}(\sigma_d/\sigma_d^c)$ ) and origin strengths ( $\log_{10}(\sigma_\lambda/\sigma_\lambda^c)$ ) of the *isw2/nhp10* mutant strain compared to the wt strain. (c,d) The replication duration of some of *S.cerevisiae* chromosomes, e.g. chr. 13 (shown in panel c) and 15 (panel d), in the mutant strain is well predicted by the bottleneck estimate rather than EVD estimate. Data of MMS (DNA alkylating agent methyl methanesulfonate) treated wild-type and *isw2 nhp10* mutant strains of *S.cerevisiae* from ref. [25]. Origin locations are obtained from the literature [6]. Origins with zero firing rate from the fit were deleted in the statistics on inter-origin distances and origin strengths.

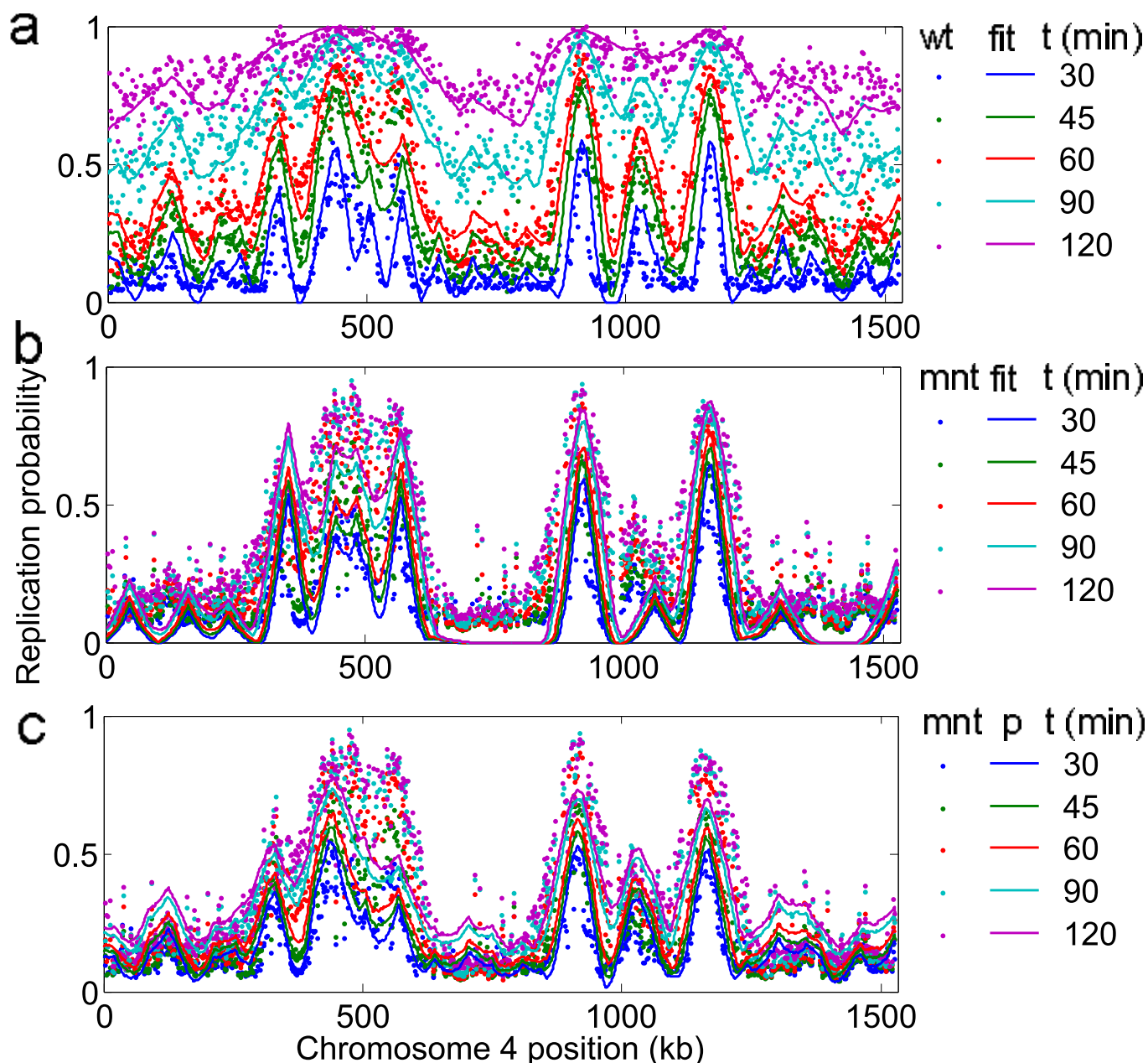


FIG. S16. The model predicts well replication timing profiles of *S. cerevisiae isw2 nhp10* mutant (mnt) strains. The plots refer to chromosome 4 as an example. Dots correspond to experimental data of MMS-treated wild-type and *isw2 nhp10* mutant strains of *S. cerevisiae* from ref. [25], and lines indicates a model fit or prediction (p). Different dot colors correspond to different times. (a) Model fit of replication timing profiles of chromosome 4 of the wt strain. Origin locations from ref. [6] were used in this fit. (b) Model fit of replication timing profiles of chromosome 4 of the *isw2 nhp10* mutant strain. (c) Model prediction of mutant replication timing profiles based on the best-fit parameters from the wt data. The model parameters correspond to best-fit values of  $\gamma$  and origin strengths from the wt data. For the prediction, all origin rates from the wt best fit were multiplied by an adjusted global constant factor (about 1/8), and fork speed and replication initial time were taken from the fit of mutant data.

TABLE S1. The parameters for genomes and chromosomes of *S.cerevisiae*, *L.kluyveri* and *S.pombe* from the best fit of genome-wide time-course replication data with the model.

Parameters for *S.cerevisiae* (SC), *L.kluyveri* and *S.pombe* genomes

Species*	$\gamma^\dagger$	$v^\dagger$	$T_0^\dagger$	$\langle d \rangle^\ddagger$	$\sigma_d^\ddagger$	$\langle \lambda \rangle^\ddagger$	$\sigma_\lambda^\ddagger$
		(kb/min)	(min)	(kb)	(kb)	( $\text{min}^{-\gamma-1}$ )	( $\text{min}^{-\gamma-1}$ )
SC wt1	1.5	1.8	1.3	26.1	16.9	$5.3 \times 10^{-4}$	$4.5 \times 10^{-4}$
SC mut1	1.5	2.0	5.0	26.2	17.2	$1.9 \times 10^{-4}$	$2.1 \times 10^{-4}$
SC wt2	0.25	0.84	-13	37.3	22.9	$3.1 \times 10^{-3}$	$2.0 \times 10^{-3}$
SC mut2	0.75	0.27	-161	85.4	64.3	$8.4 \times 10^{-5}$	$5.6 \times 10^{-5}$
<i>L.kluyveri</i>	1.75	2.5	72.5	47.0	24.6	$9.2 \times 10^{-5}$	$6.2 \times 10^{-5}$
<i>S.pombe</i>	2.0	2.55	20.1	45.0	27.9	$5.9 \times 10^{-6}$	$3.7 \times 10^{-6}$

Parameters for *S.cerevisiae* wt1 chromosomes 1-16 (c1-c16)

Parameter	c1	c2	c3	c4	c5	c6	c7	c8	c9	c10	c11	c12	c13	c14	c15	c16
n <sup>§</sup>	12	34	15	51	20	13	41	26	20	26	24	40	35	25	40	37
$\langle d \rangle$ (kb)	19.3	23.6	20.0	30.0	28.1	20.8	26.2	21.3	22.2	29.1	27.7	26.9	26.1	31.3	27.0	25.5
$\sigma_d$ (kb)	12.8	13.6	13.2	20.0	13.5	12.3	18.0	14.8	16.4	17.7	17.3	20.5	15.6	16.0	19.2	15.0
$\langle \lambda \rangle$ ( $\times 10^{-4} \text{ min}^{-2.5}$ )	4.5	4.3	5.0	6.0	6.2	4.7	5.0	4.8	4.9	5.4	5.7	5.5	5.6	5.3	5.5	5.2
$\sigma_\lambda$ ( $\times 10^{-4} \text{ min}^{-2.5}$ )	4.1	3.1	5.9	4.5	5.5	6.5	4.5	4.1	3.4	4.5	4.3	6.0	4.3	4.4	4.4	3.8

Parameters for *S.cerevisiae* mut1 chromosomes 1-16 (c1-c16)

Parameter	c1	c2	c3	c4	c5	c6	c7	c8	c9	c10	c11	c12	c13	c14	c15	c16
n	12	34	15	51	20	12	40	26	20	25	24	40	35	25	40	37
$\langle d \rangle$ (kb)	19.4	23.6	20.0	29.7	28.1	22.4	26.8	21.1	22.2	30.1	27.7	26.8	26.0	31.2	26.9	25.5
$\sigma_d$ (kb)	12.7	13.7	13.3	20.0	13.5	17.1	19.2	14.8	16.4	18.8	17.3	20.2	15.7	16.0	19.1	15.0
$\langle \lambda \rangle$ ( $\times 10^{-4} \text{ min}^{-2.5}$ )	1.7	1.5	2.8	2.0	2.7	2.2	1.8	1.7	2.2	2.2	1.7	1.9	1.9	1.7	2.1	1.5
$\sigma_\lambda$ ( $\times 10^{-4} \text{ min}^{-2.5}$ )	1.8	1.7	3.4	2.1	2.9	4.3	1.7	1.5	1.7	2.5	1.2	2.5	1.9	1.8	2.1	1.3

Parameters for *S.cerevisiae* wt2 chromosomes 1-16 (c1-c16) treated with MMS

Parameter	c1	c2	c3	c4	c5	c6	c7	c8	c9	c10	c11	c12	c13	c14	c15	c16
n	6	20	10	36	17	7	32	15	12	20	20	29	22	18	31	26
$\langle d \rangle$ (kb)	41.0	40.6	33.4	41.7	32.8	41.3	33.5	35.6	36.6	37.4	33.4	36.5	42.7	42.6	34.7	35.4
$\sigma_d$ (kb)	40.4	26.1	19.2	25.4	16.2	35.3	18.3	20.2	23.6	21.8	19.4	25.8	26.5	19.1	21.2	22.8
$\langle \lambda \rangle$ ( $\times 10^{-3} \text{ min}^{-1.25}$ )	3.4	3.0	3.6	2.7	3.3	4.4	3.0	2.8	3.7	3.5	2.6	3.2	3.6	3.0	2.9	2.8
$\sigma_\lambda$ ( $\times 10^{-3} \text{ min}^{-1.25}$ )	1.7	1.5	2.0	1.6	2.1	2.9	2.2	1.3	3.0	2.9	2.0	1.7	1.8	2.1	1.9	1.7

Parameters for *S.cerevisiae* mut2 chromosomes 1-16 (c1-c16) treated with MMS

Parameter	c1	c2	c3	c4	c5	c6	c7	c8	c9	c10	c11	c12	c13	c14	c15	c16
n	4	10	6	20	7	3	13	6	4	9	6	14	9	5	15	13
$\langle d \rangle$ (kb)	63.8	80.6	51.3	75.5	80.5	119.0	83.1	93.3	114.0	87.9	108.0	78.5	99.3	166.0	75.9	71.2
$\sigma_d$ (kb)	51.5	54.4	28.7	70.1	42.6	114.0	50.4	61.0	63.4	50.2	58.7	67.9	79.4	117.0	67.5	36.3
$\langle \lambda \rangle$ ( $\times 10^{-5} \text{ min}^{-1.75}$ )	5.2	9.2	9.4	5.2	10.0	12.2	9.1	7.9	16.4	10.5	8.9	8.1	10.1	10.2	6.9	7.2
$\sigma_\lambda$ ( $\times 10^{-5} \text{ min}^{-1.75}$ )	3.9	6.1	9.6	4.7	4.5	8.7	4.8	5.0	5.1	6.3	4.2	4.3	5.7	7.4	4.6	4.9

Continued on next page.

TABLE S1. *Continued from previous page*

Parameters for <i>L.kluyveri</i> chromosomes 1-8 (c1-c8)								
Parameter	c1	c2	c3	c4	c5	c6	c7	c8
n	24	25	27	27	30	31	43	39
$\langle d \rangle$ (kb)	42.6	44.9	46.9	49.1	43.9	44.9	41.3	59.8
$\sigma_d$ (kb)	29.0	22.6	18.0	24.4	14.1	21.1	22.0	34.4
$\langle \lambda \rangle$ ( $\times 10^{-5} \text{ min}^{-2.75}$ )	7.4	9.8	11.6	9.7	7.0	8.9	7.9	11.4
$\sigma_\lambda$ ( $\times 10^{-5} \text{ min}^{-2.75}$ )	4.6	7.1	5.7	7.1	5.1	5.3	5.9	6.8

Parameters for <i>S.pombe</i> chromosomes 1-3 (c1-c3)			
Parameter	c1	c2	c3
n	125	107	52
$\langle d \rangle$ (kb)	45.1	43.5	47.4
$\sigma_d$ (kb)	26.9	31.0	23.3
$\langle \lambda \rangle$ ( $\times 10^{-6} \text{ min}^{-3}$ )	5.5	5.0	8.5
$\sigma_\lambda$ ( $\times 10^{-6} \text{ min}^{-3}$ )	3.2	3.1	4.7

\**SC* wt1 and *SC* mut1 are the wide-type and origin mutant strains of *S.cerevisiae* respectively from Hawkins et al. [6]. *SC* wt2 and *SC* mut2 are the wide-type and *isw2nhp10* mutant strains of *S.cerevisiae* respectively from Vincent et al. [25].

† global parameters

‡ statistics of local parameters (inter-origin distances and origin strengths).

§ origin numbers of *L.kluyveri*, *S.cerevisiae* and *S.pombe* are from Agier et al. [7], Hawkins et al. [6] and Heichinger et al. [22] respectively. As for *S.cerevisiae* origin mutant, three inactivated origins were deleted from the origin list. For *S.cerevisiae isw2nhp10* mutant, origins with zero strengths were removed.